Throughput Analysis and Optimization of Wireless-Powered Multiple Antenna Full-Duplex Relay Systems

Mohammadali Mohammadi, *Member, IEEE,* Batu K. Chalise, *Senior Member, IEEE,* Himal A. Suraweera, *Senior Member, IEEE,* Caijun Zhong, *Senior Member, IEEE,* Gan Zheng, *Senior Member, IEEE,* and Ioannis Krikidis, *Senior Member, IEEE*

***Abstract*—We consider a full-duplex (FD) decode-and-forward system in which the time-switching protocol is employed by the multi-antenna relay to receive energy from the source and transmit information to the destination. The instantaneous throughput is maximized by optimizing receive and transmit beamformers at the relay and the time-split parameter. We study both optimum and suboptimum schemes. The reformulated problem in the optimum scheme achieves closed-form solutions in terms of transmit beamformer for some scenarios. In other scenarios, the optimization problem is formulated as a semi-definite relaxation problem and a rank-one optimum solution is always guaranteed. In the suboptimum schemes, the beamformers are obtained using maximum ratio combining, zero-forcing, and maximum ratio transmission. When beamformers have closed-form solutions, the achievable instantaneous and delay-constrained throughput are analytically characterized. Our results reveal that, beamforming increases both the energy harvesting and loop interference suppression capabilities at the FD relay. Moreover, simulation results demonstrate that the choice of the linear processing scheme as well as the time-split plays a critical role in determining the FD gains.**

***Index Terms*—Full-duplex, wireless power transfer, decode-and-forward relay, throughput, outage probability.**

I. Introduction

The emergence of multimedia rich wireless services coupled with ever growing number of subscribers has placed a high demand for radio resources such as bandwidth and energy. Most wireless radios so far have adopted half-duplex (HD) operation where uplink and downlink communication are "orthogonalized" in either time or frequency domain, which leads to a loss of spectral efficiency. An attractive solution to improve the spectral efficiency is to allow full-duplex (FD) simultaneous transmission/reception at the expense of loopback interference (LI) caused by the signal leakage from the transceiver output to the input [1]–[5].

Traditionally, LI suppression has been performed using passive isolation techniques such as placing RF absorber material between antennas, deploying of directional antennas. [6]. These schemes alone are inadequate to suppress the LI below the noise floor level required in most wireless systems. To achieve more effective suppression, a FD node could apply time-domain active techniques to pre-cancel the radio frequency (RF) (analog domain) or baseband (digital domain) LI signal [5], [7]. However, such mitigation schemes require sophisticated electronic implementation [4]. With the ubiquitous use of multi-antenna wireless systems, spatial domain precoding techniques can also be deployed at MIMO FD nodes. Such techniques have received significant interest as an attractive FD solution [8], [9].

On the other hand, many contemporary communication systems are battery powered and have a limited operational lifetime. To this end energy harvesting communications is a new paradigm that can power wireless devices by scavenging energy from external resources such as solar, wind, ambient RF power etc. [10]. However, energy harvesting from such sources are not without challenges due to the unpredictable nature of these energy sources. To this end, wireless energy transfer has been touted as a promising technique for a variety of wireless applications [11]–[13].

RF signals can carry both information and energy and this fundamental tradeoff has been studied in [14], [15]. In order to address practical issues associated with simultaneous information and energy transfer (same signal can not be used for both decoding and rectifying), two practical approaches, i.e., time-switching (TS) and power-splitting (PS) point-to-point system architectures were proposed in [16]. Subsequent works have also considered wireless-powered HD relay transmission with TS and PS architectures, for example, different relay networks have been studied considering amplify-and-forward (AF) and decode-and-forward (DF) relaying [19]–[21], large scale networks [22] and multiple antenna relay systems [23], [24].

Inspired by the benefits of FD and wireless power transfer,

Mohammadali Mohammadi is with the Faculty of Engineering, Shahrekord University, Shahrekord 115, Iran (email: m.a.mohammadi@eng.sku.ac.ir).

Batu K. Chalise is with Cleveland State University, 2121 Euclid Avenue, Cleveland, OH 44115 (email: b.chalise@csuohio.edu).

Himal A. Suraweera is with the Department of Electrical and Electronic Engineering, University of Peradeniya, Peradeniya 20400, Sri Lanka (email: himal@ee.pdn.ac.lk).

Caijun Zhong is with the Department of Information Science and Electronic Engineering, Zhejiang University, Hangzhou 310027, China (email: caijunzhong@zju.edu.cn).

Gan Zheng is with School of Computer Science and Electronic Engineering, University of Essex, UK (email: ganzheng@essex.ac.uk).

I. Krikidis is with the Department of Electrical and Computer Engineering, University of Cyprus, Nicosia 1678, Cyprus (email: krikidis@ucy.ac.cy).

This work was presented in part at the IEEE International Workshop on Signal Processing Advances in Wireless Communications (SPAWC 2015), Stockholm, Sweden, June/July 2015.

some recent papers have investigated the performance of wireless-powered FD point-to-point [25], [26] and relay systems [27], [28]. In [25] a wireless network model with a hybrid FD access-point (AP) that broadcasts wireless energy to a set of downlink users and at the same time receives information from the users in the uplink has been considered. In [26] software-defined radio implementation of a wireless system that transmits data and power in the same frequency has been presented. In [27], the achievable throughput of FD AF and DF relaying systems with TS has been studied. In [28] the performance of a wireless-powered AF relaying system has been also studied. The protocol in [28] considers energy harvesting from LI and therefore can recycle some part of the relay transmit energy. However, [27] and [28] only assumed single transmit/receive antennas at the relay.

Inspired by the current work on wireless-powered FD, in this paper we consider a two-hop MIMO relay system where the multiple antenna FD relay is powered via wireless energy transfer from the source. The main motivation for the adoption of multiple antennas at the relay is two-fold: (1) employment of an antenna array helps the relay to accumulate more energy (2) spatial LI cancellation techniques can be deployed. Specifically, we design receive and transmit beamformers at the relay and optimize TS parameter to characterize instantaneous as well as delay-constrained throughputs. The main contributions of the paper are summarized as follows:

1) Optimum as well as suboptimum schemes for maximizing the instantaneous throughput are proposed. In the optimum scheme, the beamformer optimization is reformulated in terms of the transmit beamformer which is shown to have closed-form solutions for some scenarios. In other scenarios where such solutions are not available, we reformulate the optimization problem as a semi-definite relaxation (SDR) problem in terms of a transmit beamforming matrix. The resulting optimization can be solved as a convex feasibility problem. We prove that the SDR problem either yields optimum rank-one solution or such solution can always be recovered from the optimum beamforming matrix solution of the SDR problem.
2) In the suboptimum schemes, we employ zero-forcing (ZF), maximum ratio combining (MRC), and maximum ratio transmission (MRT) schemes for obtaining receive and transmit beamfomers. More specifically, we solve the optimization problems that arise due to the application of transmit zero-forcing (TZF)/ MRC and MRT/receive zero-forcing (RZF) as transmit/receive beamformers.
3) In all of the above schemes, the optimum time-split parameter is analytically determined.
4) For the suboptimum schemes, which yield closed-form solutions, we develop new expressions for the system's outage probability. These expressions are helpful for investigating the effects of key system parameters on performance metrics such as the outage probability and delay-constrained throughput.
5) We present simple high signal-to-noise ratio (SNR) expressions for the outage probability of suboptimum schemes which enable the characterization of the system's diversity order and array gain.

The remainder of the paper is organized as follows: Section II presents the multiple antenna FD relay system model. Section III introduces joint transmit/receive beamforming designs. The instantaneous and delay-constrained throughput of these beamforming schemes are analyzed in Section IV and V, respectively. Numerical results are reported in Section VI. Finally, Section VII concludes the paper and summarizes the key findings.

Notation: We use bold upper case letters to denote matrices, bold lower case letters to denote vectors. $\|\cdot\|$, $(\cdot)^\dagger$, $(\cdot)^{-1}$ and $\mathtt{tr}(\cdot)$ denote the Euclidean norm, conjugate transpose operator, matrix inverse and the trace of a matrix respectively; $\mathtt{E}\{x\}$ stands for the expectation of the random variable x; $\Pr(\cdot)$ denotes the probability; $f_X(\cdot)$ and $F_X(\cdot)$ denote the probability density function (pdf) and cumulative distribution function (cdf) of the random variable (RV) X, respectively; $\mathcal{CN}(\mu,\sigma^2)$ denotes a circularly symmetric complex Gaussian RV x with mean μ and variance σ^2; $\Gamma(a)$ is the Gamma function; $\Gamma(a,x)$ is upper incomplete Gamma function [29, Eq. (8.350)]; $K_\nu(\cdot)$ is the νth order modified Bessel function of the second kind [29, Eq. (8.432)]; $\psi(x)$ is the digamma function [30, Eq. (6.3.1)]; $E_n(x)$ is the E_n-function [30, Eq. (5.1.4)] and $G_{pq}^{mn}\left(z \mid \begin{smallmatrix} a_1 \cdots a_p \\ b_1 \cdots b_q \end{smallmatrix}\right)$ denotes the Meijer G-function [29, Eq. (9.301)].

II. System Model and Problem Formulation

We consider a multiple antenna DF relay system consisting of one source S, one relay R, and one destination, D as shown in Fig. 1. Both S and D are equipped with a single antenna. To enable FD operation, R is equipped with two sets of antennas, i.e., M_R receiving antennas and M_T transmitting antennas. We assume that the S to D link does not exist.

It is also assumed that R has no external power supply, and is powered through wireless energy transfer from S as in [19], [27]. We adopt the TS protocol [16], [19], hence the entire communication process is divided into two phases, i.e., for a transmission block time T, α fraction of the block time is devoted for energy harvesting and the remaining time, $(1-\alpha)T$, is used for information transmission. It is also assumed that the channels experience Rayleigh fading and remain constant over the block time T and varies independently and identically from one block to the other.

During the energy harvesting phase, the received signal $\mathbf{r}_e$ at the relay can be expressed as

$$\mathbf{r}_e = \sqrt{\frac{P_S}{d_1^\tau}}\mathbf{h}_{SR}x_e + \mathbf{n}_R, \tag{1}$$

where P_S is the source transmit power, d_1 is the distance between the source and relay, τ is the path loss exponent,

$\mathbf{h}_{SR}$ is the $M_R \times 1$ channel vector for the S-R link,[1] i.e., input antennas at R are connected to the rectennas, x_e is the energy symbol with unit energy, and $\mathbf{n}_R$ is the additive white Gaussian noise (AWGN) at the relay with $\mathtt{E}\left\{\mathbf{n}_R\mathbf{n}_R^\dagger\right\} = \sigma_R^2\mathbf{I}_{M_R}$. As in [19], we assume that the energy harvested during the energy harvesting phase is stored in a supercapacitor and then fully consumed by R to forward the source signal to the destination. This type of operation is also known as the "harvest-use" architecture in the literature [21], [27]. We assume that the harvested energy due to the noise (including both the antenna noise and the rectifier noise) is small and thus ignored [19], [27], [31]. Hence, the relay transmit power can be written as

$$P_r = \frac{\kappa}{d_1^\tau} P_S \|\mathbf{h}_{SR}\|^2, \tag{2}$$

where $\kappa \triangleq \frac{\eta\alpha}{1-\alpha}$ and η denotes the energy conversion efficiency. Now, let us consider the information transmission phase. The received signal at R can be expressed as

$$\mathbf{r}[n] = \sqrt{\frac{P_S}{d_1^\tau}}\mathbf{h}_{SR}x_S[n] + \mathbf{H}_{RR}\mathbf{x}_R[n] + \mathbf{n}_R[n], \tag{3}$$

where $x_S[n]$ is the source information symbol with unit energy, and $\mathbf{x}_R[n]$ is the transmitted relay signal satisfying $\mathtt{E}\left\{\mathbf{x}_R[n]\mathbf{x}_R^\dagger[n]\right\} = P_r$. In order to reduce the effects of LI on system performance, a spatial interference cancellation scheme[2] is used at R and we model the $M_R \times M_T$ residual LI channel $\mathbf{H}_{RR}$ as a fading feedback channel. To this end, several residual LI channel models have been proposed in the literature, see for e.g., [3]–[5], [32], [33]. Since each implementation of a particular LI cancellation scheme can be characterized by a specific residual power, the elements of $\mathbf{H}_{RR}$ can be modeled as independent identically distributed $\mathcal{CN}(0, \sigma_{RR}^2)$ RVs, which is a common assumption in the literature since the dominant line-of-sight component in LI can be removed effectively when a propagation-domain cancellation method is implemented [5], [6]. Since R adopts the DF protocol, upon receiving the signal, it first applies a linear combining vector $\mathbf{w}_r$ on $\mathbf{r}[n]$ to obtain an estimate of x_S, then forwards the signal to D using the transmit beamforming vector $\mathbf{w}_t$. It is assumed that $\|\mathbf{w}_t\| = \|\mathbf{w}_r\| = 1$.

The relay's estimate $\hat{x}_S[n] = \mathbf{w}_r^\dagger\mathbf{r}[n]$ can be expressed as

$$\hat{x}_S[n] = \sqrt{\frac{P_S}{d_1^\tau}}\mathbf{w}_r^\dagger\mathbf{h}_{SR}x_S[n] + \mathbf{w}_r^\dagger\mathbf{H}_{RR}\mathbf{x}_R[n] + \mathbf{w}_r^\dagger\mathbf{n}_R[n]. \tag{4}$$

The relay transmit signal is given by [4]

$$\mathbf{x}_R[n] = \sqrt{P_r}\mathbf{w}_t\hat{x}_S[n-\delta], \tag{5}$$

[1]Another design choice would be to use all receive and transmit antennas during the energy harvesting phase. Analyzing this case involves different RVs in SINR expressions and left out as future work due to limited space. Moreover, as observed in single/dual antenna relay implementation [27], "receive antennas" versus "all antennas" design options are expected to follow similar trends reported in this work and achieve comparable performance depending on the operating SNR regime.

[2]Perfect estimation and cancellation of the LI is not possible due to the presence of inevitable transceiver chain impairments [4], [33] and therefore, the results reported in our paper serve as useful theoretical bounds for practical design.

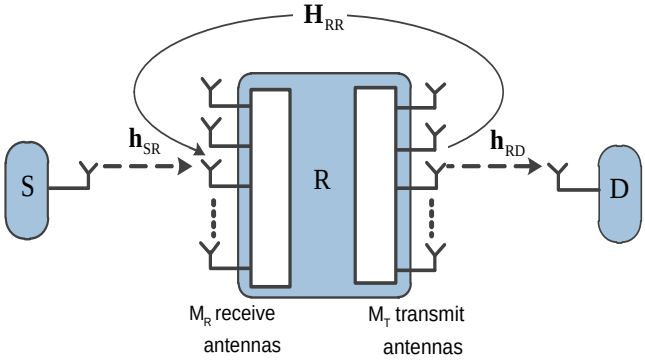

Fig. 1. Full-duplex relay system model.

where δ accounts for the time delay caused by relay processing. Finally, the received signal at D is expressed as

$$y_D[n] = \sqrt{\frac{1}{d_2^\tau}}\mathbf{h}_{RD}\mathbf{x}_R[n] + n_D[n]. \tag{6}$$

where $\mathbf{h}_{RD}$ is the $1 \times M_T$ channel vector of the $R-D$ link, d_2 is the distance between R and D and n_D denotes the AWGN at R with $\mathtt{E}\left\{n_D n_D^\dagger\right\} = \sigma_D^2$.

With the DF protocol, end-to-end SINR can be written as

$$\gamma_{\mathsf{FD}} = \min\left(\frac{\frac{\rho_1}{d_1^\tau}|\mathbf{w}_r^\dagger\mathbf{h}_{SR}|^2}{\frac{\kappa\rho_1}{d_1^\tau}\|\mathbf{h}_{SR}\|^2|\mathbf{w}_r^\dagger\mathbf{H}_{RR}\mathbf{w}_t|^2 + 1}, \frac{\kappa\rho_2}{d_1^\tau d_2^\tau}\|\mathbf{h}_{SR}\|^2|\mathbf{h}_{RD}\mathbf{w}_t|^2\right), \tag{7}$$

where $\rho_1 = \frac{P_S}{\sigma_R^2}$ and $\rho_2 = \frac{P_S}{\sigma_D^2}$.

Using (7), the system's instantaneous rate is given by

$$R(\alpha, \mathbf{w}_t, \mathbf{w}_r) = (1-\alpha)\log_2(1+\gamma_{\mathsf{FD}}). \tag{8}$$

Our objective is to maximize the rate $R(\alpha, \mathbf{w}_t, \mathbf{w}_r)$ w.r.t. α, $\mathbf{w}_t$, and $\mathbf{w}_r$. This is mathematically expressed as

$$\max_{\|\mathbf{w}_r\|=\|\mathbf{w}_t\|=1,\ \alpha\in[0,1)} R(\alpha, \mathbf{w}_t, \mathbf{w}_r). \tag{9}$$

The optimization problem (9) is nonconvex and the challenge is to obtain optimum solutions efficiently. Towards this end, in the sequel, we propose optimum and suboptimum schemes that solve (9). More specifically, in the first step, we keep α fixed and propose optimum and suboptimum schemes for beamformer design. In the second step, α is optimized for the obtained beamformers. Although this two-step optimization problem requires a joint optimization w.r.t. α and $\mathbf{w}_t$ in the optimum scheme, we show that it can still be solved efficiently.

Remark 1: Apart from data-dependent transmit power, energy consumption in the power amplifier/RF circuitry and processing power of the LI cancellation technique employed could have a significant impact on FD transceiver operation [34]. Towards this end, recent advances made with very low energy consumption micro-controllers and RF circuitry is already making it possible to use harvested power in realistic applications [35]. Nevertheless, performance analysis of wireless-powered FD transceiver operation with circuit and processing power consumption is an interesting future direction worth more research.

III. Joint Receive/Transmit Beamforming

In this section, we consider the beamforming design problem to solve the optimization problem (9) for a given α. In this case, (9) turns to a problem of maximizing the minimum two-hop SINR, which is expressed as

$$\max_{\|\mathbf{w}_r\|=\|\mathbf{w}_t\|=1} \min\left(\frac{\frac{\rho_1}{d_1^\tau}|\mathbf{w}_r^\dagger \mathbf{h}_{SR}|^2}{\frac{\kappa\rho_1}{d_1^\tau}\|\mathbf{h}_{SR}\|^2|\mathbf{w}_r^\dagger \mathbf{H}_{RR}\mathbf{w}_t|^2+1}, \frac{\kappa\rho_2}{d_1^\tau d_2^\tau}\|\mathbf{h}_{SR}\|^2|\mathbf{h}_{RD}\mathbf{w}_t|^2\right). \quad (10)$$

In the following subsections, we propose optimum as well as different suboptimum schemes for solving (10). In the optimum approach, we propose SDR problem but show that relaxation does not change the optimality of the solution, whereas in the suboptimum schemes, different linear receiver/transmitter techniques are employed at R.

A. Optimum Scheme

Since the second-hop SNR does not depend on $\mathbf{w}_r$, we can maximize the first-hop SINR w.r.t $\mathbf{w}_r$ by fixing $\mathbf{w}_t$. In this case, the optimization problem (10) is re-formulated as

$$\max_{\|\mathbf{w}_r\|=1} \frac{|\mathbf{w}_r^\dagger \mathbf{h}_{SR}|^2}{\frac{\kappa\rho_1}{d_1^\tau}\|\mathbf{h}_{SR}\|^2|\mathbf{w}_r^\dagger \mathbf{H}_{RR}\mathbf{w}_t|^2+1}, \quad (11)$$

which is a generalized Rayleigh ratio problem [36]. It is well known that (11) is globally maximized when

$$\mathbf{w}_r = \frac{\left(\frac{\kappa\rho_1}{d_1^\tau}\|\mathbf{h}_{SR}\|^2\mathbf{H}_{RR}\mathbf{w}_t\mathbf{w}_t^\dagger\mathbf{H}_{RR}^\dagger+\mathbf{I}\right)^{-1}\mathbf{h}_{SR}}{\left\|\left(\frac{\kappa\rho_1}{d_1^\tau}\|\mathbf{h}_{SR}\|^2\mathbf{H}_{RR}\mathbf{w}_t\mathbf{w}_t^\dagger\mathbf{H}_{RR}^\dagger+\mathbf{I}\right)^{-1}\mathbf{h}_{SR}\right\|}. \quad (12)$$

Accordingly, by substituting $\mathbf{w}_r$ into (11) and applying the Sherman Morrison formula [37], the first term inside the min operator in (10) is obtained as

$$\begin{aligned}\psi &\triangleq \frac{\rho_1}{d_1^\tau}\left(\mathbf{h}_{SR}^\dagger\left(\frac{\kappa\rho_1\|\mathbf{h}_{SR}\|^2}{d_1^\tau}\mathbf{H}_{RR}\mathbf{w}_t\mathbf{w}_t^\dagger\mathbf{H}_{RR}^\dagger+\mathbf{I}\right)^{-1}\mathbf{h}_{SR}\right)\\ &= \frac{\rho_1}{d_1^\tau}\left(\|\mathbf{h}_{SR}\|^2-\frac{\frac{\kappa\rho_1\|\mathbf{h}_{SR}\|^2}{d_1^\tau}|\mathbf{h}_{SR}^\dagger\mathbf{H}_{RR}\mathbf{w}_t|^2}{1+\frac{\kappa\rho_1\|\mathbf{h}_{SR}\|^2}{d_1^\tau}\|\mathbf{H}_{RR}\mathbf{w}_t\|^2}\right). \quad (13)\end{aligned}$$

Now, the optimization problem in (10) is re-expressed as

$$\max_{\|\mathbf{w}_t\|=1} \min\left(\frac{\rho_1}{d_1^\tau}\left(\|\mathbf{h}_{SR}\|^2-\frac{\frac{\kappa\rho_1}{d_1^\tau}\|\mathbf{h}_{SR}\|^2|\mathbf{h}_{SR}^\dagger\mathbf{H}_{RR}\mathbf{w}_t|^2}{1+\frac{\kappa\rho_1}{d_1^\tau}\|\mathbf{h}_{SR}|^2\|\mathbf{H}_{RR}\mathbf{w}_t\|^2}\right), \frac{\kappa\rho_2}{d_1^\tau d_2^\tau}\|\mathbf{h}_{SR}\|^2|\mathbf{h}_{RD}\mathbf{w}_t|^2\right), \quad (14)$$

which is still difficult to solve due to its nonconvex nature.

One of the key results of the optimum scheme is presented in the following proposition.

Proposition 1: The optimal $\mathbf{w}_{t,o}$ is given by

$$\mathbf{w}_{t,o} = \begin{cases}\mathbf{w}_{\mathsf{mSINR}}, & \text{if} \quad f_1(\mathbf{w}_{\mathsf{mSINR}}) \le f_2(\mathbf{w}_{\mathsf{mSINR}})\\ \mathbf{w}_{\mathsf{MRT}}, & \text{if} \quad f_2(\mathbf{w}_{\mathsf{MRT}}) \le f_1(\mathbf{w}_{\mathsf{MRT}})\\ \mathbf{w}_t \text{ is obtained from the feasibility problem } \mathcal{P}, & \text{otherwise}\end{cases} \quad (15)$$

where

$$\begin{aligned}f_1(\mathbf{w}_t) &= \frac{\rho_1}{d_1^\tau}\left(\|\mathbf{h}_{SR}\|^2-\frac{\frac{\kappa\rho_1}{d_1^\tau}\|\mathbf{h}_{SR}\|^2|\mathbf{h}_{SR}^\dagger\mathbf{H}_{RR}\mathbf{w}_t|^2}{1+\frac{\kappa\rho_1}{d_1^\tau}\|\mathbf{h}_{SR}\|^2\|\mathbf{H}_{RR}\mathbf{w}_t\|^2}\right)\\ f_2(\mathbf{w}_t) &= \frac{\kappa\rho_2}{d_1^\tau d_2^\tau}\|\mathbf{h}_{SR}\|^2|\mathbf{h}_{RD}\mathbf{w}_t|^2\end{aligned}$$

$$\begin{aligned}\mathbf{w}_{\mathsf{mSINR}} &= \max_{\mathbf{w}_t} f_1(\mathbf{w}_t)\\ &= \min_{\mathbf{w}_t} \frac{\frac{\kappa\rho_1}{d_1^\tau}\|\mathbf{h}_{SR}\|^2\mathbf{w}_t^\dagger\mathbf{H}_{RR}^\dagger\mathbf{h}_{SR}\mathbf{h}_{SR}^\dagger\mathbf{H}_{RR}\mathbf{w}_t}{\mathbf{w}_t^\dagger\left(\mathbf{I}+\frac{\kappa\rho_1}{d_1^\tau}\|\mathbf{h}_{SR}\|^2\mathbf{H}_{RR}^\dagger\mathbf{H}_{RR}\right)\mathbf{w}_t}\\ \mathbf{w}_{\mathsf{MRT}} &= \max_{\mathbf{w}_t} f_2(\mathbf{w}_t) = \frac{\mathbf{h}_{RD}^\dagger}{||\mathbf{h}_{RD}||},\\ &\quad t \in \left[0, \min\left(\frac{\rho_1}{d_1^\tau}||\mathbf{h}_{SR}||^2, \frac{\kappa\rho_2}{d_1^\tau d_2^\tau}\|\mathbf{h}_{SR}\|^2||\mathbf{h}_{RD}||^2\right)\right]\end{aligned}$$

and $\mathcal{P}$ is

$$\begin{aligned}\mathcal{P}: \quad &\text{Find } \mathbf{W}_t, y\\ \text{s.t.} \quad &ty \le \frac{\rho_1}{d_1^\tau}\left(\|\mathbf{h}_{SR}\|^2 y - \frac{\kappa\rho_1}{d_1^\tau}\|\mathbf{h}_{SR}\|^2\mathbf{h}_{SR}^\dagger\mathbf{H}_{RR}\mathbf{W}_t\mathbf{H}_{RR}^\dagger\mathbf{h}_{SR}\right)\\ &y = \mathsf{tr}\left(\mathbf{W}_t\left(\mathbf{I}+\frac{\kappa\rho_1}{d_1^\tau}\|\mathbf{h}_{SR}\|^2\mathbf{H}_{RR}^\dagger\mathbf{H}_{RR}\right)\right)\\ &t \le \frac{\kappa\rho_2}{d_1^\tau d_2^\tau}\|\mathbf{h}_{SR}\|^2\mathbf{h}_{RD}\mathbf{W}_t\mathbf{h}_{RD}^\dagger\\ &\mathsf{tr}\left(\mathbf{W}_t\right)=1, \mathbf{W}_t \succeq 0. \quad (16)\end{aligned}$$

The maximum value of t for which the problem $\mathcal{P}$ is feasible gives the relaxed optimum solution $\mathbf{W}_t$.

Proof: Note that $\mathbf{w}_{\mathsf{mSINR}}$ is the eigenvector corresponding to the minimum eigenvalue of the matrix $(\mathbf{I}+\frac{\kappa\rho_1}{d_1^\tau}\|\mathbf{h}_{SR}\|^2\mathbf{H}_{RR}^\dagger\mathbf{H}_{RR})^{-1}(\mathbf{H}_{RR}^\dagger\mathbf{h}_{SR}\mathbf{h}_{SR}^\dagger\mathbf{H}_{RR})$. The solution of $\mathbf{w}_t$ that maximizes $f_1(\mathbf{w}_t)$ is $\mathbf{w}_{\mathsf{mSINR}}$, whereas $f_2(\mathbf{w}_t)$ is maximized by $\mathbf{w}_{\mathsf{MRT}}$. Now consider the following cases:

- $f_1(\mathbf{w}_{\mathsf{mSINR}}) \le f_2(\mathbf{w}_{\mathsf{mSINR}})$: In this case the two possible scenarios for $\mathbf{w}_t \ne \mathbf{w}_{\mathsf{mSINR}}$ are $f_1(\mathbf{w}_t) \le f_2(\mathbf{w}_t)$ and $f_1(\mathbf{w}_t) > f_2(\mathbf{w}_t)$. In the former case, $\min(f_1(\mathbf{w}_t), f_2(\mathbf{w}_t)) = f_1(\mathbf{w}_t)$ but it follows that $f_1(\mathbf{w}_t) \le f_2(\mathbf{w}_{\mathsf{mSINR}})$ since $f_1(\mathbf{w}_t) \le f_1(\mathbf{w}_{\mathsf{mSINR}})$. In the latter case, $\min(f_1(\mathbf{w}_t), f_2(\mathbf{w}_t)) = f_2(\mathbf{w}_t)$ but it follows that $f_2(\mathbf{w}_t) \le f_1(\mathbf{w}_{\mathsf{mSINR}}) \le f_2(\mathbf{w}_{\mathsf{mSINR}})$. Therefore, $\mathbf{w}_{\mathsf{mSINR}}$ is the optimum precoder when $f_1(\mathbf{w}_{\mathsf{mSINR}}) \le f_2(\mathbf{w}_{\mathsf{mSINR}})$.
- $f_2(\mathbf{w}_{\mathsf{MRT}}) \le f_1(\mathbf{w}_{\mathsf{MRT}})$: The two possible scenarios are $f_2(\mathbf{w}_t) \le f_1(\mathbf{w}_t)$ and $f_2(\mathbf{w}_t) > f_1(\mathbf{w}_t)$ where $\mathbf{w}_t \ne \mathbf{w}_{\mathsf{MRT}}$. In the former case, $\min(f_1(\mathbf{w}_t), f_2(\mathbf{w}_t)) = f_2(\mathbf{w}_t)$ but it follows that $f_2(\mathbf{w}_t) \le f_1(\mathbf{w}_{\mathsf{MRT}})$ since $f_2(\mathbf{w}_t) \le f_2(\mathbf{w}_{\mathsf{MRT}})$. In the latter case, $\min(f_1(\mathbf{w}_t), f_2(\mathbf{w}_t)) = f_1(\mathbf{w}_t)$ but it follows that $f_1(\mathbf{w}_t) \le f_2(\mathbf{w}_{\mathsf{MRT}}) \le f_1(\mathbf{w}_{\mathsf{MRT}})$. Therefore, $\mathbf{w}_{\mathsf{MRT}}$ is the optimum precoder when $f_2(\mathbf{w}_{\mathsf{MRT}}) \le f_1(\mathbf{w}_{\mathsf{MRT}})$.
- For remaining cases, to the best of our knowledge, there is no closed-form solution for the optimization problem (14). Introducing an auxiliary variable $t \ge 0$, (14) is

expressed as

$$\max_{\|\mathbf{w}_t\|=1, t} \quad t$$
$$\text{s.t.} \quad t \le \frac{\rho_1}{d_1^\tau}\left(\|\mathbf{h}_{SR}\|^2 - \frac{\frac{\kappa\rho_1}{d_1^\tau}\|\mathbf{h}_{SR}\|^2|\mathbf{h}_{SR}^\dagger\mathbf{H}_{RR}\mathbf{w}_t|^2}{1+\frac{\kappa\rho_1}{d_1^\tau}\|\mathbf{h}_{SR}\|^2\|\mathbf{H}_{RR}\mathbf{w}_t\|^2}\right)$$
$$t \le \frac{\kappa\rho_2}{d_1^\tau d_2^\tau}\|\mathbf{h}_{SR}\|^2|\mathbf{h}_{RD}\mathbf{w}_t|^2. \quad (17)$$

This is a nonconvex quadratic optimization problem with nonconvex constraint. To solve the problem in (17), we first apply SDR technique by using a positive-semidefinite matrix $\mathbf{W}_t = \mathbf{w}_t\mathbf{w}_t^\dagger$ and relaxing the rank-constraint on $\mathbf{W}_t$. Moreover, define the auxiliary variable

$$y = \mathsf{tr}\left(\mathbf{W}_t\left(\mathbf{I} + \frac{\kappa\rho_1}{d_1^\tau}\|\mathbf{h}_{SR}\|^2\mathbf{H}_{RR}^\dagger\mathbf{H}_{RR}\right)\right).$$

The relaxed optimization problem (17) in terms of $\mathbf{W}_t$, y, and t is

$$\max_{\mathbf{W}_t, t, y} \quad t$$
$$\text{s.t.} \quad ty \le \frac{\rho_1}{d_1^\tau}\left(\|\mathbf{h}_{SR}\|^2 y - \frac{\kappa\rho_1}{d_1^\tau}\|\mathbf{h}_{SR}\|^2\mathbf{h}_{SR}^\dagger\mathbf{H}_{RR}\mathbf{W}_t\mathbf{H}_{RR}^\dagger\mathbf{h}_{SR}\right)$$
$$y = \mathsf{tr}\left(\mathbf{W}_t\left(\mathbf{I} + \frac{\kappa\rho_1}{d_1^\tau}\|\mathbf{h}_{SR}\|^2\mathbf{H}_{RR}^\dagger\mathbf{H}_{RR}\right)\right)$$
$$t \le \frac{\kappa\rho_2}{d_1^\tau d_2^\tau}\|\mathbf{h}_{SR}\|^2\mathbf{h}_{RD}\mathbf{W}_t\mathbf{h}_{RD}^\dagger$$
$$\mathsf{tr}(\mathbf{W}_t) = 1, \mathbf{W}_t \succeq 0. \quad (18)$$

The optimization problem (18) is still nonconvex. However, for a given t, the problem turns to a convex feasibility problem given in (16). We show that there is no need to solve this feasibility problem for all possible values of t. This can be demonstrated as follows. Note that the constraints of the problem (18) show that t can be upper bounded as $t \le \min\left(\frac{\rho_1}{d_1^\tau}||\mathbf{h}_{SR}^2||^2, \frac{\kappa\rho_2}{d_1^\tau d_2^\tau}\|\mathbf{h}_{SR}\|^2||\mathbf{h}_{RD}||^2\right)$. Consequently, we can start solving the feasibility problem (16) in the decreasing order for t. The largest value of t for which the problem is feasible yields the optimum $\mathbf{W}_t$. If the optimum $\mathbf{W}_t$ is rank-one, then the relaxed problem (18) is equivalent to the original problem. ■

In the following, we show that the relaxed optimization (18) or convex feasibility problem (16) provides an optimum rank-one solution. To this end, we present another key result of the optimum scheme in the following proposition.

Proposition 2: The rank-one optimum $\mathbf{W}_t$ can always be guaranteed in (18).

Proof: The proof is based on Karush-Kuhn-Tucker (KKT) conditions and given in Appendix I. ■

B. TZF Scheme

We now present some suboptimum beamforming solutions. The first is the TZF scheme, where relay takes advantage of the multiple transmit antennas to completely cancel the LI [8]. To ensure this is feasible, the number of the transmit antennas at relay should be greater than one, i.e., $M_T > 1$. In addition, MRC is applied at the relay input, i.e., $\mathbf{w}_r = \frac{\mathbf{h}_{SR}}{\|\mathbf{h}_{SR}\|}$. After substituting $\mathbf{w}_r$ into (10), the optimal transmit beamforming vector $\mathbf{w}_t$ is obtained by solving the following problem:

$$\max_{\|\mathbf{w}_t\|=1} \quad |\mathbf{h}_{RD}\mathbf{w}_t|^2$$
$$\text{s.t.} \quad \mathbf{h}_{SR}^\dagger\mathbf{H}_{RR}\mathbf{w}_t = 0. \quad (19)$$

We know that $\mathbf{A} \triangleq \mathbf{H}_{RR}^\dagger\mathbf{h}_{SR}\mathbf{h}_{SR}^\dagger\mathbf{H}_{RR}$ is a rank-one Hermitian matrix with eigenvalue $\lambda \triangleq \|\mathbf{h}_{SR}^\dagger\mathbf{H}_{RR}\|^2$ and eigenvector $\mathbf{x} \triangleq \frac{\mathbf{H}_{RR}^\dagger\mathbf{h}_{SR}}{||\mathbf{H}_{RR}^\dagger\mathbf{h}_{SR}||}$. Consequently, the eigenvalue decomposition of $\mathbf{A}$ can be given by $\mathbf{x}^\dagger\left(\mathbf{I} - \frac{1}{\lambda}\mathbf{A}\right) = \mathbf{0}$ which implies that $\mathbf{x}^\dagger\left(\mathbf{I} - \frac{1}{\lambda}\mathbf{A}\right)\bar{\mathbf{w}}_t = 0$ for all $\bar{\mathbf{w}}_t \neq \mathbf{0}$. Comparing this with the ZF constraint in (19), it is clear that we can take $\mathbf{w}_t = \mathbf{B}\bar{\mathbf{w}}_t$, where $\mathbf{B} \triangleq \mathbf{I} - \frac{\mathbf{H}_{RR}^\dagger\mathbf{h}_{SR}\mathbf{h}_{SR}^\dagger\mathbf{H}_{RR}}{\|\mathbf{h}_{SR}^\dagger\mathbf{H}_{RR}\|^2}$, without violating the ZF constraint. As such, the objective function in (19) reduces to $|\mathbf{h}_{RD}\mathbf{B}\bar{\mathbf{w}}_t|^2$ which is maximized with $\bar{\mathbf{w}}_t = k_c\mathbf{B}\mathbf{h}_{RD}^\dagger$. Since $||\mathbf{w}_t|| = 1$ and $\mathbf{B} = \mathbf{B}^2$, it is clear that $k_c = \frac{1}{||\mathbf{B}\mathbf{h}_{RD}^\dagger||}$. Consequently, the transmit beamformer for the TZF scheme is given by

$$\mathbf{w}_t^{\mathsf{ZF}} = \frac{\mathbf{B}\mathbf{h}_{RD}^\dagger}{\|\mathbf{B}\mathbf{h}_{RD}^\dagger\|}. \quad (20)$$

C. RZF Scheme

As an alternative solution, the transmit beamforming vector can be set using the MRT principle, i.e., $\mathbf{w}_t = \frac{\mathbf{h}_{RD}^\dagger}{\|\mathbf{h}_{RD}\|}$, and $\mathbf{w}_r$ is designed with the ZF criterion $\mathbf{w}_r^\dagger\mathbf{H}_{RR}\mathbf{w}_t = 0$. To ensure feasibility of RZF, R should be equipped with $M_R > 1$ receive antennas. Substituting the MRT solution for $\mathbf{w}_t$ into (10), the optimal receive beamforming vector $\mathbf{w}_r$ is the solution of the following problem:

$$\max_{\|\mathbf{w}_r\|=1} \quad |\mathbf{w}_r^\dagger\mathbf{h}_{SR}|^2$$
$$\text{s.t.} \quad \mathbf{w}_r^\dagger\mathbf{H}_{RR}\mathbf{h}_{RD}^\dagger = 0. \quad (21)$$

Using similar steps as in the TZF scheme, the optimal combining vector $\mathbf{w}_r$ is obtained as

$$\mathbf{w}_r^{\mathsf{ZF}} = \frac{\mathbf{D}\mathbf{h}_{SR}}{\|\mathbf{D}\mathbf{h}_{SR}\|}, \quad (22)$$

where $\mathbf{D} \triangleq \mathbf{I} - \frac{\mathbf{H}_{RR}\mathbf{h}_{RD}^\dagger\mathbf{h}_{RD}\mathbf{H}_{RR}^\dagger}{\|\mathbf{H}_{RR}\mathbf{h}_{RD}\|^2}$.

D. MRC/MRT Scheme

Finally, we consider the MRC/MRT scheme, where $\mathbf{w}_r$ and $\mathbf{w}_t$ are set to match the first hop and second hop channel, respectively. Hence,

$$\mathbf{w}_r^{\mathsf{MRC}} = \frac{\mathbf{h}_{SR}^\dagger}{\|\mathbf{h}_{SR}\|}, \quad \mathbf{w}_t^{\mathsf{MRT}} = \frac{\mathbf{h}_{RD}^\dagger}{\|\mathbf{h}_{RD}\|}. \quad (23)$$

It is worthwhile to note that the optimum, TZF, and RZF schemes reduce to the MRC/MRT scheme in the absence of LI. Although the MRC/MRT scheme is not optimal in the presence of LI, it could be favored in situations where compatibility with HD systems is a concern. Moreover, as we

show in Section VI, the MRC/MRT scheme exhibits a very good performance as compared to other schemes under mild LI effect. Note that the MRC/MRT scheme requires only the knowledge of $\mathbf{h}_{SR}$ and $\mathbf{h}_{RD}$, whereas the other three schemes require the knowledge of $\mathbf{h}_{SR}$, $\mathbf{h}_{RD}$, and $\mathbf{H}_{RR}$.

IV. Optimizing α for Instantaneous Throughput

In this section, we optimize α for the FD beamforming schemes proposed in the previous section and maximize the instantaneous throughput which is given by [27]

$$R_{\mathsf{I}}(\alpha) = (1-\alpha)\log_2(1+\gamma_{\mathsf{FD}}). \tag{24}$$

This expression reveals an interesting trade-off between the duration of energy harvesting and the instantaneous throughput. A longer energy harvesting time increases the harvested energy and consequently the second hop SNR, however decreases the available time for information transmission and vice-versa. Therefore, an appropriate system design can optimize the instantaneous throughput by adjusting α.

A. Optimum Scheme

Substituting the optimum $\mathbf{w}_{t,o}$, the instantaneous rate as a function of α is

$$\begin{aligned} R_{\mathrm{Opt}}(\alpha) = (1-\alpha)\log_2\Big(1+\|\mathbf{h}_{SR}\|^2 \\ \times \min\left(\frac{\rho_1}{d_1^\tau}\left(1-\frac{\frac{\kappa\rho_1}{d_1^\tau}|\mathbf{h}_{SR}^\dagger\mathbf{H}_{RR}\mathbf{w}_{t,o}|^2}{1+\frac{\kappa\rho_1}{d_1^\tau}\|\mathbf{h}_{SR}\|^2\|\mathbf{H}_{RR}\mathbf{w}_{t,o}\|^2}\right), \right. \\ \left.\left.\frac{\kappa\rho_2}{d_1^\tau d_2^\tau}|\mathbf{h}_{RD}\mathbf{w}_{t,o}|^2\right)\right). \end{aligned} \tag{25}$$

Let $b_0 = \frac{\rho_2}{\rho_1}\frac{\eta}{d_2^\tau}|\mathbf{h}_{RD}\mathbf{w}_{t,o}|^2$, $b_1 = \frac{\eta\rho_1}{d_1^\tau}|\mathbf{h}_{SR}^\dagger\mathbf{H}_{RR}\mathbf{w}_{t,o}|^2$, and $b_2 = \frac{\eta\rho_1}{d_1^\tau}\|\mathbf{h}_{SR}\|^2\|\mathbf{H}_{RR}\mathbf{w}_{t,o}\|^2$. Hence, (25) is written as

$$\begin{aligned} R_{\mathrm{Opt}}(\alpha) = (1-\alpha)\log_2\left(1+\frac{\rho_1}{d_1^\tau}\|\mathbf{h}_{SR}\|^2\right. \\ \left.\times\min\left(1-\frac{\frac{\alpha b_1}{1-\alpha}}{1+\frac{\alpha b_2}{1-\alpha}}, \frac{\alpha b_0}{1-\alpha}\right)\right). \end{aligned} \tag{26}$$

Thus, the optimal α is obtained by solving

$$\alpha_{\mathrm{Opt}}^* = \arg\max_{0<\alpha<1} R_{\mathrm{opt}}(\alpha). \tag{27}$$

Denote $f = \frac{\rho_1}{d_1^\tau}\|\mathbf{h}_{SR}\|^2$ and $\tilde{f} = fb_0$. The above optimization problem can be solved analytically as shown in the following proposition.

Proposition 3: The optimal α_{Opt}^* is given by

$$\alpha_{\mathrm{Opt}}^* = \begin{cases} \frac{e^{W\left(\frac{\tilde{f}-1}{e}\right)+1}-1}{\tilde{f}-1+e^{W\left(\frac{\tilde{f}-1}{e}\right)+1}}, & \text{if} \quad e^{W\left(\frac{\tilde{f}-1}{e}\right)+1} < \alpha_0\tilde{f}+1; \\ \frac{\alpha_0}{1+\alpha_0}, & \text{otherwise,} \end{cases} \tag{28}$$

where $W(x)$ is the Lambert W function in which $W(x)$ is the solution of $W\exp(W) = x$ and noting that $b_1 \le b_2$ from Cauchy-Schwarz inequality, α_0 is given by

$$\alpha_0 = \frac{(b_2-b_1-b_0)+\sqrt{b_0^2+(b_2-b_1)^2+2b_0(b_1+b_2)}}{2b_0b_2}.$$

Proof: The following two cases are considered:

1) if $\frac{\alpha b_0}{1-\alpha} < 1-\frac{\frac{\alpha b_1}{1-\alpha}}{1+\frac{\alpha b_2}{1-\alpha}}$ or $\alpha < \frac{\alpha_0}{1+\alpha_0}$, we have
$$R_{\mathrm{Opt}}(\alpha) = (1-\alpha)\log_2\left(1+\frac{\alpha}{1-\alpha}\tilde{f}\right).$$
Therefore, taking the first order derivative of $R_{\mathrm{Opt}}(\alpha)$ with respect to α, and using the procedure described in [27], the optimal time portion α can be obtained as
$$\alpha_{\mathrm{Opt}}^* = \frac{e^{W(\frac{\tilde{f}-1}{e})+1}-1}{\tilde{f}-1+e^{W(\frac{\tilde{f}-1}{e})+1}}. \tag{29}$$
2) Otherwise, if $\alpha > \frac{\alpha_0}{1+\alpha_0}$, the instantaneous throughput in (26) is given by
$$R_{\mathrm{Opt}}(\alpha) = (1-\alpha)\log_2\left(1+f\left(1-\frac{\alpha b_1}{1-\alpha+\alpha b_2}\right)\right).$$
Taking the first derivative of $R_{\mathrm{Opt}}(\alpha)$ with respect to α yields
$$\begin{aligned}\frac{dR_{\mathrm{Opt}}(\alpha)}{d\alpha} = &-\log_2\left(1+f\left(1-\frac{\alpha b_1}{1-\alpha+\alpha b_2}\right)\right) \\ &-\frac{(1-\alpha)fb_1}{(1-\alpha+\alpha b_2)^2\log 2}\frac{1}{1+f\left(1-\frac{\alpha b_1}{1-\alpha+\alpha b_2}\right)},\end{aligned}$$
which is strictly smaller than zero. Therefore, $R_{\mathrm{Opt}}(\alpha)$ is a decreasing function with respect to α, and hence the optimal α is given by
$$\alpha_{\mathrm{Opt}}^* = \frac{\alpha_0}{1+\alpha_0}. \tag{30}$$

■

B. TZF Scheme

Substituting $\mathbf{w}_t^{\mathsf{ZF}}$ into (7), the instantaneous throughput of the TZF scheme is given by

$$\begin{aligned} R_{\mathsf{I},\mathsf{TZF}}(\alpha) = (1-\alpha)\log_2\left(1+\min\left(\frac{\rho_1}{d_1^\tau}\|\mathbf{h}_{SR}\|^2,\right.\right. \\ \left.\left.\frac{\kappa\rho_2}{d_1^\tau d_2^\tau}\|\mathbf{h}_{SR}\|^2\|\mathbf{B}\mathbf{h}_{RD}\|^2\right)\right). \end{aligned} \tag{31}$$

Hence, the optimal α can be obtained by solving the following optimization problem

$$\alpha_{\mathsf{TZF}}^* = \arg\max_{0<\alpha<1} R_{\mathsf{I},\mathsf{TZF}}(\alpha). \tag{32}$$

In (32), since $R_{\mathsf{I},\mathsf{TZF}}(\alpha)$ is concave with respect to α, α_{TZF}^* can be obtained by solving the equation $\frac{dR_{\mathsf{I},\mathsf{TZF}}(\alpha)}{d\alpha} = 0$. Using the similar approach as in the optimum scheme, α_{TZF}^* can be derived as

$$\alpha_{\mathsf{TZF}}^* = \begin{cases} \frac{e^{W\left(\frac{a_1-1}{e}\right)+1}-1}{a_1-1+e^{W\left(\frac{a_1-1}{e}\right)+1}}, & \text{if} \quad e^{W\left(\frac{a_1-1}{e}\right)+1} < \frac{a_1}{\alpha_1}+1; \\ \frac{1}{1+\alpha_1}, & \text{otherwise,} \end{cases} \tag{33}$$

where $a_1 = \frac{\eta\rho_2}{d_1^\tau d_2^\tau}\|\mathbf{h}_{SR}\|^2\|\mathbf{B}\mathbf{h}_{RD}\|^2$, $a_2 = \frac{d_1^\tau}{\rho_1\|\mathbf{h}_{SR}\|^2}$, and $\alpha_1 = a_1a_2$.

C. RZF Scheme

Substituting $\mathbf{w}_r^{\mathsf{ZF}}$ into (7), the instantaneous throughput of the RZF scheme can be written as

$$\begin{aligned} R_{\mathsf{I},\mathsf{RZF}}(\alpha) = (1-\alpha)\log_2\left(1+\min\left(\frac{\rho_1}{d_1^\tau}\|\mathbf{D}\mathbf{h}_{SR}\|^2,\right.\right. \\ \left.\left.\frac{\kappa\rho_2}{d_1^\tau d_2^\tau}\|\mathbf{h}_{SR}\|^2\|\mathbf{h}_{RD}\|^2\right)\right). \end{aligned} \tag{34}$$

Accordingly, the optimal α can be obtained as

$$\alpha^*_{\mathsf{RZF}} = \begin{cases} \frac{e^{W\left(\frac{a_3-1}{e}\right)+1}-1}{a_3-1+e^{W\left(\frac{a_1-1}{e}\right)+1}}, & \text{if} \quad e^{W\left(\frac{a_3-1}{e}\right)+1} < \frac{a_3}{\alpha_2}+1; \\ \frac{1}{1+\alpha_2}, & \text{otherwise}, \end{cases} \tag{35}$$

where $a_3 = \frac{\eta\rho_2}{d_1^\tau d_2^\tau}\|\mathbf{h}_{SR}\|^2\|\mathbf{h}_{RD}\|^2$, $a_4 = \frac{d_1^\tau}{\rho_1\|\mathbf{D}\mathbf{h}_{SR}\|^2}$, and $\alpha_2 = a_3a_4$.

D. MRC/MRT Scheme

Substituting $\mathbf{w}_r^{\mathsf{MRC}}$ and $\mathbf{w}_t^{\mathsf{MRT}}$ into (7), the instantaneous throughput of the MRC/MRT scheme can be expressed as

$$R_{\mathsf{I,MRC}}(\alpha) = (1-\alpha)\log_2\left(1+\min\left(\frac{\frac{\rho_1}{d_1^\tau}\|\mathbf{h}_{SR}\|^2}{\frac{\kappa\rho_1}{d_1^\tau}\|\mathbf{h}_{SR}\|^2\frac{|\boldsymbol{h}_{SR}^\dagger\boldsymbol{H}_{RR}\boldsymbol{h}_{RD}^\dagger|^2}{\|\boldsymbol{h}_{SR}\boldsymbol{h}_{RD}\|^2}+1}, \frac{\kappa\rho_2}{d_1^\tau d_2^\tau}\|\mathbf{h}_{SR}\|^2\|\mathbf{h}_{RD}\|^2\right)\right). \tag{36}$$

For the notational convenience, we denote $b_3 = \frac{\rho_2}{d_1^\tau d_2^\tau}\|\mathbf{h}_{SR}\|^2\|\mathbf{h}_{RD}\|^2$, $b_4 = \frac{\rho_2}{d_1^\tau d_2^\tau}|\boldsymbol{h}_{SR}^\dagger\boldsymbol{H}_{RR}\boldsymbol{h}_{RD}^\dagger|^2$, and $b_5 = \frac{\rho_2}{\rho_1}\frac{1}{d_2^\tau}\|\boldsymbol{h}_{RD}\|^2$. Hence, (36) can be written as

$$R_{\mathsf{I,MRC}}(\alpha) = (1-\alpha)\log_2\left(1+b_3 \times \min\left(\frac{1}{\frac{\eta\alpha}{1-\alpha}b_4+b_5}, \frac{\eta\alpha}{1-\alpha}\right)\right). \tag{37}$$

As such, the optimal time-split α is the solution of the following problem:

$$\alpha^*_{\mathsf{MRC}} = \arg\max_{0<\alpha<1} R_{\mathsf{I,MRC}}(\alpha). \tag{38}$$

The above optimization problem can be solved analytically, and we have the following key result.

Proposition 4: The optimal α^*_{MRC} is given by

$$\alpha^*_{\mathsf{MRC}} = \begin{cases} \frac{e^{W\left(\frac{a_3-1}{e}\right)+1}-1}{a_3-1+e^{W\left(\frac{a_3-1}{e}\right)+1}}, & \text{if} \quad e^{W\left(\frac{a_3-1}{e}\right)+1} < \frac{a_3}{\alpha_3}+1; \\ \frac{1}{1+\alpha_3}, & \text{otherwise}, \end{cases} \tag{39}$$

where $\alpha_3 = \frac{2\eta b_4}{-b_5+\sqrt{b_5^2+4b_4}}$.

Proof: We consider two cases as follows:

1) if $\frac{\eta\alpha}{1-\alpha} < \frac{1}{\frac{\eta\alpha}{1-\alpha}b_4+b_5}$ or $\alpha < \frac{1}{1+\alpha_3}$, we have

$$R_{\mathsf{I,MRC}}(\alpha) \quad = \quad (1-\alpha)\log_2\left(1+\frac{\eta\alpha}{1-\alpha}b_3\right).$$

Therefore, taking the first order derivative of $R_{\mathsf{I,MRC}}(\alpha)$ with respect to α, and following the same procedure as in optimum scheme, the optimal time portion α can be obtained as

$$\alpha^* \quad = \quad \frac{e^{W\left(\frac{a_3-1}{e}\right)+1}-1}{a_3-1+e^{W\left(\frac{a_3-1}{e}\right)+1}}, \tag{40}$$

where $a_3 = \frac{\eta\rho_2}{d_1^\tau d_2^\tau}\|\mathbf{h}_{SR}\|^2\|\mathbf{h}_{RD}\|^2 = \eta b_3$.

2) Otherwise, if $\alpha > \frac{1}{1+\alpha_3}$, the instantaneous throughput in (37) is given by

$$R_{\mathsf{I,MRC}}(\alpha) = (1-\alpha)\log_2\left(1+\frac{b_3}{\frac{\eta\alpha}{1-\alpha}b_4+b_5}\right).$$

Taking the first derivative of $R_{\mathsf{I,MRC}}(\alpha)$ with respect to α yields

$$\frac{dR_{\mathsf{I,MRC}}(\alpha)}{d\alpha} = -\log_2\left(1+\frac{b_3}{\frac{\eta\alpha}{1-\alpha}b_4+b_5}\right) - \frac{(1-\alpha)\eta b_3 b_4}{\left(\frac{\eta\alpha}{1-\alpha}b_4+b_5\right)\left(\frac{\eta\alpha}{1-\alpha}b_4+b_5+b_3\right)\log 2}.$$

which is strictly smaller than zero. Therefore, $R_{\mathsf{I,MRC}}(\alpha)$ is a decreasing function with respect to α, and hence the optimal α is given by

$$\alpha^* \quad = \quad \frac{1}{1+\alpha_3} \tag{41}$$

■

We end this section with the following remarks. In contrast to the suboptimum schemes, the obtained solution of $\mathbf{w}_t$ in optimum scheme depends on α. As a consequence, joint optimization w.r.t. α and $\mathbf{w}_t$ is required in the latter scheme. There are two ways to solve this joint optimization. The first way is to find $\mathbf{w}_t$ by following Proposition 1 and next performing a one-dimensional line search over $0 < \alpha < 1$. This guarantees the global optimum solutions for α and $\mathbf{w}_t$. Another way is to employ an iterative approach where each iteration step consists of a two-step optimization, i.e., optimizing $\mathbf{w}_t$ for a given α and vice-versa. In either way, the computational complexity of the proposed optimum scheme is limited due to the following facts. As seen from Proposition 1, there is a need to solve SDR problem only for a specific scenario. Moreover, the rank-one optimum solution can always be recovered from optimum $\mathbf{W}_t$ which is obtained by solving the convex feasibility problem $\mathcal{P}$ in a few number of iterations. Also α can be obtained analytically for a given $\mathbf{w}_t$ or only a one-dimensional search is required for finding the optimum α. Despite these facts, the computational complexity of the optimum scheme is higher than that of the suboptimum schemes. This may be justified since, depending on the scenarios, the optimum scheme significantly outperforms the suboptimum schemes (see Fig. 2).

We outline the proposed optimum scheme for the instantaneous throughput maximization problem in Algorithm 1.

V. Delay-constrained Throughput

We now consider the delay-constrained scenario, where the source transmits at a constant rate R_c bits/sec/Hz. Due to the time variation of the fading channel, outage events where the instantaneous channel capacity is below the source transmission rate may occur. Hence, the average throughput can be computed as [19]

$$R_{\mathsf{D}}(\alpha) = (1-\mathsf{P}_{\mathsf{out}})R_c(1-\alpha), \tag{42}$$

where $\mathsf{P}_{\mathsf{out}}$ is the outage probability, which is defined as the probability that the instantaneous SINR falls below a predefined threshold, γ_{th}. Mathematically, it can be written as

$$\mathsf{P}_{\mathsf{out}} = \Pr(\gamma_{\mathsf{FD}} < \gamma_{\mathsf{th}}) = F_\gamma(\gamma_{\mathsf{th}}), \tag{43}$$

$$F_{\gamma_{\mathsf{TZF}}^{\infty}}(z) \approx \begin{cases} \left(\frac{1}{\Gamma(M_R+1)} + \frac{1}{\Gamma(M_T-1)\Gamma(M_R)} \sum_{k=0}^{\infty} \frac{(-1)^{k+1}}{k!(k+M_T)} \left(\frac{\sigma_D^2}{\sigma_R^2} \frac{d_2^\tau}{\kappa} \right)^{M_T+k-1} \frac{1}{M_R-M_T-k+1} \right) \left(\frac{d_1^\tau z}{\rho_1} \right)^{M_R}, & M_T > M_R+1, \\ \frac{1}{\Gamma(M_R+1)} \left(1 + \frac{1}{\Gamma(M_R)} \left(\ln(\rho_1) - \ln(d_1^\tau z) + \psi(1) \right) \left(\frac{\sigma_D^2}{\sigma_R^2} \frac{d_2^\tau}{\kappa} \right)^{M_R} \right) \left(\frac{d_1^\tau z}{\rho_1} \right)^{M_R}, & M_T = M_R+1, \\ \frac{\Gamma(M_R-M_T+1)}{\Gamma(M_T)\Gamma(M_R)} \left(\frac{d_2^\tau}{\kappa} \right)^{M_T-1} \left(\frac{d_1^\tau z}{\rho_2} \right)^{M_T-1}, & M_T < M_R+1. \end{cases} \quad (47)$$

Algorithm 1 The proposed optimum scheme for the instantaneous throughput maximization.

Step 1: Initialize α:
Choose α from its grid (Line search Method -LS) or generate an initial point for α (Alternating optimization method-AO) where $\alpha \in [0, 1)$.

Step 2: Obtain the transmit beamformer $\mathbf{w}_{t,\mathrm{o}}$ using (15).
if (15) requires solving the feasibility problem $\mathcal{P}$ of (16) **then**
if $\mathbf{W}_{\mathrm{t}}$ is rank-one **then**
Take $\mathbf{w}_{t,\mathrm{o}}$ as the eigenvector corresponding to non-zero eigenvalue of $\mathbf{W}_{\mathrm{t}}$.
else
Take $\mathbf{w}_{t,\mathrm{o}}$ as given in *Case b* of the Appendix I (see (82))
end if
end if

Step 4:
if AO method **then**
while not converged **do**
Obtain α_{Opt} from (28) using $\mathbf{w}_{t,\mathrm{o}}$ obtained in **Step 2**.
Update α as $\alpha = \alpha_{\mathrm{Opt}}$ and go to **Step 2**.
end while
Save $\mathbf{w}_{t,\mathrm{o}}$, α, and the objective function.
else if LS method **then**
Save $\mathbf{w}_{t,\mathrm{o}}$, α, and the objective function.
Take another α from its grid, and repeat **Step 1**.
end if

Step 3: Choose the $\mathbf{w}_{t,\mathrm{o}}$ and α that give maximum objective value.

where $\gamma_{\mathsf{th}} = 2^{R_c} - 1$. Therefore in order to find the delay-constrained throughput, the remaining key task is to characterize the exact outage probability of the system. In the sequel, we investigate the outage probability of the considered TZF, RZF, and MRC/MRT schemes. In addition, simple high SNR approximations are presented, which provide a concise characterization of the diversity order, and enable a performance comparison of these three schemes. Derivation of the outage probability of the optimum scheme is difficult. Hence we have resorted to simulations for evaluating the delay-constrained throughput of the optimum scheme in Section VI.

A. TZF Scheme

Substituting the $\mathbf{w}_t^{\mathsf{ZF}}$ and $\mathbf{w}_r^{\mathsf{MRC}}$ into (7), the end-to-end SNR γ_{TZF} can be expressed as

$$\gamma_{\mathsf{TZF}} = \frac{\rho_1 \|\boldsymbol{h}_{SR}\|^2}{(1-\alpha) d_1^\tau} \min\left(1-\alpha, \frac{\rho_2}{\rho_1} \frac{\eta\alpha}{d_2^\tau} \|\tilde{\boldsymbol{h}}_{RD}\|^2 \right), \quad (44)$$

where $\tilde{\boldsymbol{h}}_{RD}$ is an $(M_T - 1) \times 1$ vector. $\|\tilde{\boldsymbol{h}}_{RD}\|^2$ follows the chi-square distribution with $(M_T - 1)$ degrees of freedom, denoted as $\|\tilde{\boldsymbol{h}}_{RD}\|^2 \sim \chi^2_{2(M_T-1)}$ [38]. Let $Y_1 = \min\left(1-\alpha, \frac{\rho_2}{\rho_1} \frac{\eta\alpha}{d_2^\tau} \|\tilde{\boldsymbol{h}}_{RD}\|^2\right)$. The cdf of Y_1 is given by [24, Appendix II]

$$F_{Y_1}(y) = \begin{cases} 1 & y > 1-\alpha, \\ 1 - \frac{\Gamma\left(M_T-1, \frac{\rho_1}{\rho_2} \frac{y d_2^\tau}{\eta\alpha}\right)}{\Gamma(M_T-1)} & y < 1-\alpha. \end{cases} \quad (45)$$

Therefore, the cdf of γ_{TZF} can be obtained as

$$F_{\gamma_{\mathsf{TZF}}}(z) = 1 - \frac{1}{\Gamma(M_R)} \int_{\frac{d_1^\tau z}{\rho_1}}^{\infty} Q\left(M_T - 1, \frac{d_1^\tau d_2^\tau}{\kappa\rho_2} \frac{z}{x} \right) \times x^{M_R-1} e^{-x} dx, \quad (46)$$

where $Q(a, x) = \Gamma(a, x)/\Gamma(a)$.

To the best of the authors's knowledge, the integral in (46) does not admit a closed-form expression. However, (46) can be evaluated numerically.

To gain further insights, we now look into the high SNR regime and derive a simple approximation for the outage probability, which enables the characterization of the achievable diversity order of the TZF scheme.

Proposition 5: In the high SNR regime, i.e., $\rho_1, \rho_2 \to \infty$, the outage probability of the TZF scheme can be approximated as (47) at the top of the page.

Proof: See Appendix B. ∎

By inspecting (47), we see that the TZF scheme achieves a diversity order of $\min(M_R, M_T - 1)$. This is intuitive since one degree of freedom is used for interference cancellation. Moreover, we notice that for the case $M_R + 1 = M_T$, $F_{\gamma_{\mathsf{TZF}}^{\infty}}(z)$ decays as $\rho_1^{-M_R} \ln(\rho_1)$ rather than $\rho_1^{-M_R}$ as in the conventional case, which implies that in the energy harvesting case the slope of $F_{\gamma_{\mathsf{TZF}}^{\infty}}(z)$ converges much slower compared with that in the constant power case.

B. RZF Scheme

Invoking (7), and using $\mathbf{w}_r^{\mathsf{ZF}}$ and $\mathbf{w}_t^{\mathsf{MRT}}$, the end-to-end SNR γ_{RZF} can be expressed as

$$\begin{aligned} \gamma_{\mathsf{RZF}} &= \min\left(\frac{\rho_1}{d_1^\tau} \mathbf{h}_{SR}^\dagger \mathbf{D} \mathbf{h}_{SR}, \frac{\kappa\rho_2}{d_1^\tau d_2^\tau} \|\mathbf{h}_{SR}\|^2 \|\mathbf{h}_{RD}\|^2 \right) \\ &= \min\left(\frac{\rho_2}{d_1^\tau} \hat{\mathbf{h}}_{SR}^\dagger \mathsf{diag}(0, 1, \cdots, 1) \hat{\mathbf{h}}_{SR}, \frac{\kappa\rho_1}{d_1^\tau d_2^\tau} \|\mathbf{h}_{SR}\|^2 \|\mathbf{h}_{RD}\|^2 \right) \\ &= \min\left(\frac{\rho_1}{d_1^\tau} \|\tilde{\mathbf{h}}_{SR}\|^2, \frac{\kappa\rho_2}{d_1^\tau d_2^\tau} \|\mathbf{h}_{SR}\|^2 \|\mathbf{h}_{RD}\|^2 \right), \end{aligned} \quad (47)$$

where $\hat{\mathbf{h}}_{SR} = \boldsymbol{\Phi} \mathbf{h}_{SR}$ with $\boldsymbol{\Phi}$ is a unitary matrix, and $\tilde{\mathbf{h}}_{SR}$ is a $(M_R - 1) \times 1$ vector, consisting of the $M_R - 1$

last element of $\hat{\mathbf{h}}_{SR}$. In (47), the first equality follows from the fact that $\mathbf{D}$ is idempotent and the second equality is due to the eigen decomposition. Let us denote $Z_1 \triangleq \frac{1}{d_1^\tau}\left(\|\tilde{\boldsymbol{h}}_{SR}\|^2 + |\tilde{h}_1|^2\right)$ where $\hat{h}_1$ is the first element of the $\hat{\mathbf{h}}_{SR}$ and $X_1 = \frac{\|\tilde{\boldsymbol{h}}_{SR}\|^2}{\|\tilde{\boldsymbol{h}}_{SR}\|^2+|\tilde{h}_1|^2}$. Therefore, the end-to-end SINR can be re-expressed as

$$\gamma_{\mathsf{RZF}} = Z_1 \min\left(\rho_1 X_1, \frac{\kappa\rho_2}{d_2^\tau}\|\boldsymbol{h}_{RD}\|^2\right). \tag{48}$$

It is well known that Z_1 follows central chi-square distribution with $2M_R$ degrees-of-freedom, denoted as $Z_1 \sim \chi^2_{2M_R}$ and that X_1 follows a beta distribution with shape parameters M_R-1 and 1, denoted as $X_1 \sim \mathsf{Beta}(M_R-1, 1)$, with [38]

$$F_{X_1}(x) = x^{M_R-1}, \quad 0 < x < 1. \tag{49}$$

Moreover, let $Y_2 = \frac{\kappa\rho_2}{d_2^\tau}\|\boldsymbol{h}_{RD}\|^2$; we have $F_{Y_2}(y) = P\left(M_T, \frac{d_2^\tau}{\kappa\rho_2}y\right)$, where $P(a,x) = \gamma(a,x)/\Gamma(a)$. With $F_{X_1}(x)$ and $F_{Y_2}(y)$ in hand, $F_{\gamma_{\mathsf{RZF}}}(z)$ can be expressed as

$$\begin{aligned} F_{\gamma_{\mathsf{RZF}}}(z) = 1 - Q\left(M_R, \frac{d_1^\tau z}{\rho_1}\right) + \\ \frac{1}{\Gamma(M_R)}\left(\int_{\frac{d_1^\tau z}{\rho_1}}^{\infty} P\left(M_T, \frac{d_1^\tau d_2^\tau}{\kappa\rho_2}\frac{z}{x}\right) x^{M_R-1}e^{-x}dx \right. \\ \left. + \left(\frac{d_1^\tau z}{\rho_1}\right)^{M_R-1} \int_{\frac{d_1^\tau z}{\rho_1}}^{\infty} Q\left(M_T, \frac{d_1^\tau d_2^\tau}{\kappa\rho_2}\frac{z}{x}\right) e^{-x}dx\right). \end{aligned} \tag{50}$$

Although (50) does not admit a closed-form solution, it can be efficiently evaluated numerically. Now, we look into the high SNR regime, and investigate the diversity order.

Proposition 6: In the high SNR regime, i.e., $\rho_1, \rho_2 \to \infty$, the outage probability of the RZF scheme can be approximated as

$$F^{\infty}_{\gamma_{\mathsf{RZF}}}(z) \approx \begin{cases} \frac{1}{\Gamma(M_R)}\left(\frac{d_1^\tau z}{\rho_1}\right)^{M_R-1}, & M_R < M_T+1, \\ \frac{1}{\Gamma(M_R)}\left(1+\frac{1}{\Gamma(M_T+1)}\left(\frac{\sigma_D^2}{\sigma_R^2}\frac{d_2^\tau}{\kappa}\right)^{M_T}\right)\left(\frac{d_1^\tau z}{\rho_1}\right)^{M_T}, & M_R = M_T+1, \\ \frac{\Gamma(M_R-M_T)}{\Gamma(M_R)\Gamma(M_T+1)}\left(\frac{d_2^\tau}{\kappa}\right)^{M_T}\left(\frac{d_1^\tau z}{\rho_2}\right)^{M_T}, & M_R > M_T+1. \end{cases} \tag{51}$$

Proof: See Appendix C. ∎

Proposition 6 indicates that the RZF scheme achieves a diversity order of $\min(M_R-1, M_T)$. This result is also intuitively satisfying since one degree-of-freedom should be allocated for LI cancellation at the receive side of R.

C. MRC/MRT Scheme

The outage probability analysis of the MRC/MRT scheme for arbitrary M_T and M_R appears to be cumbersome. Therefore, we now consider two special cases as follows: Case-1) $M_T = 1$, $M_R \geq 1$ and Case-2) $M_T \geq 1$, $M_R = 1$.

Case-1): In this case $\frac{|\boldsymbol{h}_{SR}^\dagger \boldsymbol{H}_{RR}\boldsymbol{h}_{RD}^\dagger|^2}{\|\boldsymbol{h}_{SR}\boldsymbol{h}_{RD}\|^2}$ is given by

$$X_2 \triangleq |\mathbf{w}_r^{\mathsf{MRC}}\boldsymbol{h}_{RR}|^2 = \frac{|\,\hat{\boldsymbol{h}}_{SR,1}\,|^2}{\|\boldsymbol{h}_{SR}\|^2}\|\boldsymbol{h}_{RR}\|^2. \tag{52}$$

For notational convenience, we define $c_1 = \frac{\rho_1}{d_1^\tau}$, $c_2 = \frac{\kappa\rho_1\sigma_{RR}^2}{d_1^\tau}$, $c_3 = \frac{\kappa\rho_2}{d_1^\tau d_2^\tau}$. Then, the end-to-end SINR can be re-expressed as

$$\gamma_{\mathsf{MRC}} = \min\left(\frac{c_1\|\boldsymbol{h}_{SR}\|^2}{c_2|\hat{\boldsymbol{h}}_{SR,1}|^2\|\boldsymbol{h}_{RR}\|^2+1}, c_3\|\boldsymbol{h}_{SR}\|^2|h_{RD}|^2\right). \tag{53}$$

Let us denote $X = c_1/\left(c_2X_2 + \frac{1}{Y_3}\right)$ where $X2 = \frac{|\hat{\boldsymbol{h}}_{SR,1}|^2\|\boldsymbol{h}_{RR}\|^2}{\|\boldsymbol{h}_{SR}\|^2}$ and $Y = c_3Y_3Y_4$, with $Y_3 = \|\boldsymbol{h}_{SR}\|^2$ and $Y_4 = |h_{RD}|^2$. Accordingly, the cdf of γ^{MRC} in (53) can be expressed as

$$\begin{aligned} F_{\gamma_{\mathsf{MRC}}}(z) &= \Pr(\min(X,Y) < z), \\ &= 1 - \Pr(X > z, Y > z). \end{aligned} \tag{54}$$

Conditioned on Y_3, the RVs X and Y are independent and hence we have

$$\begin{aligned} &\Pr(X > z, Y > z) \\ &= \int_{\frac{d_1^\tau z}{\rho_1}}^{\infty}\left(1 - F_{X|Y_3}(z)\right)\left(1 - F_{Y|Y_3}(z)\right) f_{Y_3}(y)dy, \\ &= \int_{\frac{d_1^\tau z}{\rho_1}}^{\infty} F_{X_2}\left(\frac{1}{c_2}\left(\frac{c_1}{z} - \frac{1}{y}\right)\right)\left(1 - F_{Y_4}\left(\frac{z}{c_3 y}\right)\right) f_{Y_3}(y)dy. \end{aligned} \tag{55}$$

In order to evaluate (55) we require the cdf of the RV, X_2. Note that $\|\boldsymbol{h}_{RR}\|^2 \sim \chi^2_{2M_R}$, $Z_2 \triangleq \frac{|\hat{\boldsymbol{h}}_{SR,1}|^2}{\|\boldsymbol{h}_{SR}\|^2}$ is distributed as $Z_2 \sim \mathsf{Beta}(1, M_R-1)$ [38], and the cdf of X_2 can be readily evaluated as

$$\begin{aligned} F_{X_2}(t) &= \int_0^1 F_{\|\boldsymbol{h}_{RR}\|^2}\left(\frac{t}{z}\right) f_{Z_2}(z)dz, \\ &\overset{(a)}{=} \frac{1}{\Gamma(M_R-1)}\int_1^{\infty} z^{-M_R}(z-1)^{M_R-2}\gamma\left(M_R, zt\right)dz, \\ &\overset{(b)}{=} G_{23}^{21}\left(t \;\middle|\; \begin{matrix} 1, M_R \\ 1, M_R, 0 \end{matrix}\right), \end{aligned} \tag{56}$$

where $\gamma(a,x) = \Gamma(a) - \Gamma(a,x)$. The equality (a) in (56) follows by substituting $x = 1/z$ and (b) is obtained by using the identity $\gamma(c,x) = G_{12}^{11}\left(x \;\middle|\; \begin{matrix} 1 \\ c, 0 \end{matrix}\right)$ and applying the integral identity [29, Eq. (7.811.3)]. Now, using the cdf of RV Y_3, and substituting (56) into (55) we obtain

$$\begin{aligned} F_{\gamma_{\mathsf{MRC}}}(z) = 1 - \frac{1}{\Gamma(M_R)} \\ \times\int_{\frac{d_1^\tau z}{\rho_1}}^{\infty} G_{23}^{21}\left(\frac{1}{c_2}\left(\frac{c_1}{z} - \frac{1}{y}\right) \;\middle|\; \begin{matrix} 1, M_R \\ 1, M_R, 0 \end{matrix}\right) y^{M_R-1}e^{-\left(y + \frac{z}{c_3 y}\right)}dy. \end{aligned} \tag{57}$$

To the best of the authors' knowledge, the integral in (57) does not admit a closed-form solution. However, (57) can be evaluated numerically. We now look into the high SNR regime to gain more insights. To this end, neglecting the noise term of the first term inside in minimum function in (53), we write

$$\gamma^{\mathsf{low}}_{\mathsf{MRC}} > \gamma_{\mathsf{MRC}} = \min\left(\frac{1}{\kappa X_2}, \frac{\kappa\rho_2}{d_1^\tau d_2^\tau}\parallel \boldsymbol{h}_{SR} \parallel^2 |h_{RD}|^2\right). \tag{58}$$

We now present the following proposition.

Proposition 7: In the high SNR regime, i.e., $\rho_1, \rho_2 \to \infty$, with $M_T = 1$ the outage probability of the MRC/MRT

scheme can be approximated as

$$F_{\gamma_{\mathsf{MRC}}^{\mathsf{low}}}(z) = 1 - \frac{2}{\Gamma(M_R)} G_{23}^{21}\left(\frac{1}{\kappa\sigma_{RR}^2 z} \;\middle|\; \begin{matrix} 1, M_R \\ 1, M_R, 0 \end{matrix}\right) \times \left(\frac{d_1^\tau d_2^\tau}{\rho_2 \kappa} z\right)^{\frac{M_R}{2}} K_{M_R}\left(2\sqrt{\frac{d_1^\tau d_2^\tau}{\rho_2\kappa} z}\right). \quad (59)$$

Proof: See Appendix D. ∎

Moreover, by applying a Bessel function approximation for small arguments [30, Eq. (9.6.9)], in (59) we can write

$$F_{\gamma_{\mathsf{MRC}}^{\mathsf{low}}}(z) \to 1 - G_{23}^{21}\left(\frac{1}{\kappa\sigma_{RR}^2 z} \;\middle|\; \begin{matrix} 1, M_R \\ 1, M_R, 0 \end{matrix}\right). \quad (60)$$

Note that (60) presents the outage probability floor and indicates that the MRC/MRT scheme with $M_T = 1$ exhibits a zero-diversity order behavior in presence of residual LI.

Case-2) In this case $\frac{|\boldsymbol{h}_{SR}^\dagger \boldsymbol{H}_{RR} \boldsymbol{h}_{RD}^\dagger|^2}{\|\boldsymbol{h}_{SR}\boldsymbol{h}_{RD}\|^2}$ simplifies to

$$Y_5 \triangleq |\boldsymbol{h}_{RR}\boldsymbol{w}_t^{\mathsf{MRT}}|^2 = (\boldsymbol{h}_{RR}\boldsymbol{\Phi}_t \mathsf{diag}\{1, 0, \cdots, 0\}\boldsymbol{\Phi}_t^\dagger \boldsymbol{h}_{RR}^\dagger) = |\hat{\boldsymbol{h}}_{RR,1}|^2, \quad (61)$$

where $\boldsymbol{\Phi}_t$ is an unitary matrix and follows from eigen decomposition and $\hat{\boldsymbol{h}}_{RR} = \boldsymbol{h}_{RR}\boldsymbol{\Phi}_t$. Hence, γ_{MRC} can be written as

$$\gamma_{\mathsf{MRC}} = \min\left(\frac{c_1|h_{SR}|^2}{c_2|h_{SR}|^2|\hat{\boldsymbol{h}}_{RR,1}|^2 + 1}, c_3|h_{SR}|^2\|\boldsymbol{h}_{RD}\|^2\right). \quad (62)$$

Let us define $U = \frac{c_1 X_3}{c_2 X_3 Y_5 + 1}$ and $V = c_3 X_3 Y_6$, where $X_3 = |h_{SR}|^2$, $Y_6 = \|\boldsymbol{h}_{RD}\|^2$. Note that conditioned on X_3, the RVs, U and V are independent and hence we have

$$\begin{aligned} F_{\gamma_{\mathsf{MRC}}}(z) &= 1 - \int_{\frac{d_1^\tau z}{\rho_1}}^{\infty} \big(1 - F_{U|X_3}(z)\big)\big(1 - F_{V|X_3}(z)\big) f_{X_3}(x)dx, \\ &= 1 - \int_{\frac{d_1^\tau z}{\rho_1}}^{\infty} \left(1 - e^{-\frac{1}{c_2 x}\left(\frac{c_1 x}{z} - 1\right)}\right) Q\left(M_T, \frac{z}{c_3 x}\right) e^{-x} dx. \end{aligned} \quad (63)$$

Having obtained the exact outage probability expression, we now look into the high SNR regime and establish the following asymptotic outage probability approximation.

Proposition 8: In the high SNR regime, i.e., $\rho_1, \rho_2 \to \infty$, with $M_R = 1$, the outage probability of the MRC/MRT scheme can be approximated as

$$F_{\gamma_{\mathsf{MRC}}^{\infty}}(z) \approx 1 - \left(1 - e^{-\frac{1}{\kappa\sigma_{RR}^2 z}}\right) \times \left(e^{-\frac{d_1^\tau z}{\rho_1}} - \frac{1}{\Gamma(M_T)} \frac{d_1^\tau z}{\rho_1} \sum_{k=0}^{\infty} \frac{(-1)^k}{k!(M_T + k)} \times \left(\frac{\rho_1}{\rho_2}\frac{d_2^\tau}{\kappa}\right)^{M_T + k} E_{M_T + k}\left(\frac{d_1^\tau z}{\rho_1}\right)\right). \quad (64)$$

Proof: Note that in the high SNR regime, i.e., $\rho_1, \rho_2 \to \infty$, the cdf $F_{\gamma^{\mathsf{MRC}}}(z)$ can be approximated as

$$F_{\gamma_{\mathsf{MRC}}^{\infty}}(z) \approx 1 - \frac{\left(1 - e^{-\frac{c_1}{c_2 z}}\right)}{\Gamma(M_T)} \int_{\frac{d_1^\tau z}{\rho_1}}^{\infty} \Gamma\left(M_T, \frac{z}{c_3 x}\right) e^{-x} dx. \quad (65)$$

Now applying [29, Eq. (8.354.2)] and using the definition of the E_n-function we can easily obtain the desired result. ∎

In most cases, $k = 0$ is sufficient for accurate results leading to the following compact expression

$$F_{\gamma_{\mathsf{MRC}}^{\infty}}(z) \approx 1 - \left(1 - e^{-\frac{1}{\kappa\sigma_{RR}^2}\frac{1}{z}}\right)\left(e^{-\frac{d_1^\tau z}{\rho_1}} - \frac{1}{\Gamma(M_T + 1)} \times \left(\frac{\rho_1}{\rho_2}\frac{d_2^\tau}{\kappa}\right)^{M_T} \frac{d_1^\tau z}{\rho_1} E_{M_T}\left(\frac{d_1^\tau z}{\rho_1}\right)\right), \quad (66)$$

while in other cases it can be truncated using few terms up to 10.

At this point, it is important to determine the value of α that maximizes the throughput. We note that delay-constrained throughput should converge to the ceiling value of $R_c(1-\alpha)$ when $\mathsf{P}_{\mathsf{out}} \to 0$. For each beamforming scheme we observe that $\mathsf{P}_{\mathsf{out}}$ is a complicated function of α and it decreases as the value of α is increased. However, this will lead to the decrease of the term $(1 - \alpha)$ at the same time. Therefore, an optimal value of α that maximizes the delay-constrained throughput exists and it can be found by solving the following optimization problem [27, Eq. (18)]

$$\alpha^* = \arg\max_{0<\alpha<1} R(\alpha). \quad (67)$$

Given (46), (50), (57) and (63), unfortunately the optimization problem in (67) does not admit closed-form solutions. However, the optimal α^* can be solved numerically.

VI. Numerical Results and Discussion

We now present numerical results based on analytical expressions developed and investigate the impact of key system parameters on the performance. The simulations adopt parameters of the 3GPP LTE for small cell deployments [39]. The maximum transmit power of the source node is set to 26 dBm. The energy conversion efciency is set to be $\eta = 0.5$.[3]

A. Instantaneous Throughput

We consider the influence of optimal time-split α and LI effect on the instantaneous throughput of different beamforming schemes. Fig. 2 shows the instantaneous throughput versus α of the beamforming schemes for a single time frame and channel realizations. There are two groups of curves: the OPA (dashed line) and EPA (solid line) curves. OPA and EPA refer to the cases where source allocates different and equal power levels for energy harvesting phase and the information transmission phase respectively. The results for OPA have been obtained using a two dimentional grid search stratergy over α and the splitting factor that controls the source power for the energy harvesting phase and the information transmission phase. It is clear that the OPA scheme achieves a higher throughput than the EPA scheme over the entire range of the time-split. We can see that the values of the optimal α calculated by (28), (33), (35), and (39) coincide with the corresponding ones obtained via simulation. Also, as expected, the optimum scheme outperforms all other schemes on all time-split values. In addition, simulation results, not

[3]We note that the typical values for practical parameters used in EH systems will depend on both the system application and specific technology used for implementation of RF energy harvesting circuits.

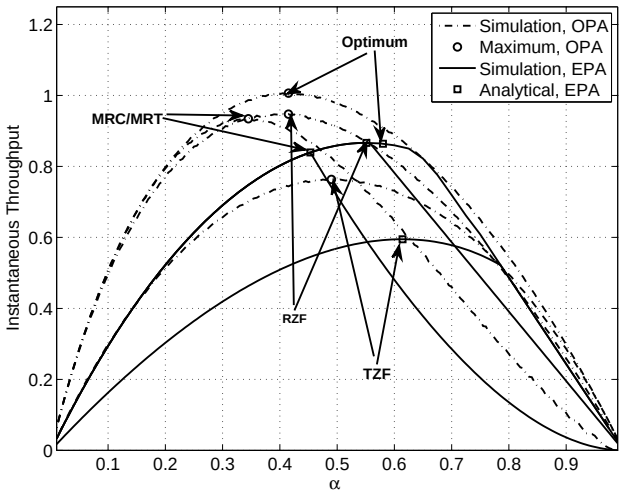

Fig. 2. Instantaneous throughput versus α for proposed beamforming schemes ($M_T = M_R = 3$, $P_S = 20$ dBm, $d_1 = 20$, $d_2 = 10$ and $\tau = 3$).

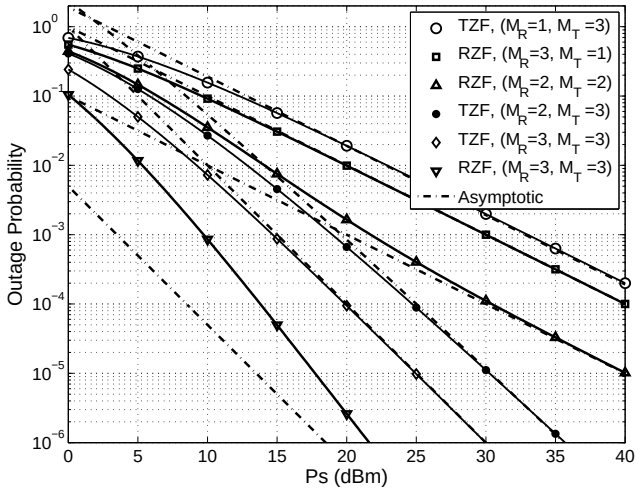

Fig. 3. Outage probability versus P_S of the TZF and RZF schemes for different antenna configurations.

shown in the figure to avoid clutter, reveal that the values of the optimal α decrease as either the number of relays' receive antennas or the sources' transmit power increases. This is because in these cases the relay node can harvest the same amount of energy in a shorter time. Therefore, more time must be allocated to the information transmission phase in order to improve the system throughput.

B. Outage Probability

Fig. 3 shows the outage probability for the ZF based beamforming schemes with different antenna configurations and for a specific $\alpha = 0.5$ and $d_1 = d_2 = 10$ m. The asymptotic results based on (47) and (51) are also presented. Since the relay is capable of canceling LI, we see that the outage probability of the TZF and RZF beamforming schemes decays proportionally to the diversity orders reported in Proposition 5 and 6, respectively. Comparing the TZF and RZF schemes with the same diversity orders and different receive antenna numbers (i.e., TZF, with $M_R = 1$ and $M_T = 3$, and RZF with $M_R = 3$ and $M_T = 1$) we see that the additional receive antenna could harvest more energy

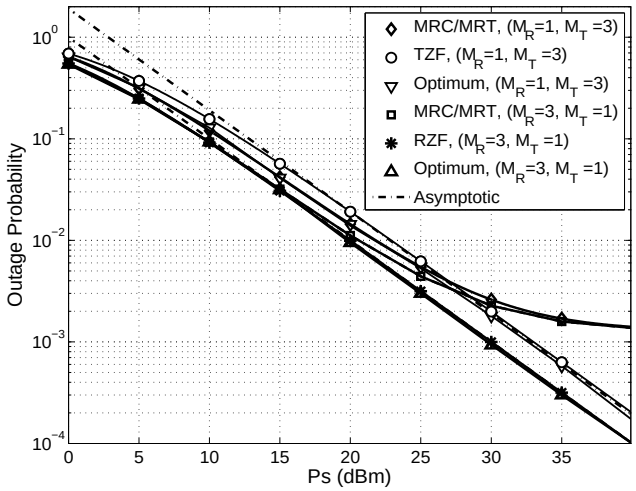

Fig. 4. Outage probability versus P_S of the optimum, TZF, RZF, MRC/MRT schemes for different antenna configurations.

to increase the second-hop SNR and to facilitate information transfer. Moreover, for the case where $M_R = M_T$, RZF achieves a higher array gain. This observation demonstrates that while under some configurations ($M_T = 1$) or ($M_R = 1$) only one form (receive or transmit) of beamforming design can be implemented, when both designs can be applied, the system designer has to carefully decide on the configuration as well as the beamforming design.

Fig. 4 compares the outage probability of the optimum, TZF, RZF, and MRC/MRT schemes with different antenna configurations and for $\alpha = 0.5$ and $d_1 = d_2 = 10$ m. The residual LI strength at the relay is set to be -50 dBm. Asymptotic results in (59) and (66) are also provided for the MRC/MRT scheme. The outage performance of the MRC/MRT scheme is almost identical to the optimum scheme at low SNRs, while the ZF-based schemes can achieve almost the same performance of the optimum scheme in the high SNR regime. When the transmit power increases and α remains fixed, an excessive amount of energy will be collected at the relay, which is detrimental for the MRC/MRT scheme since it results in a strong LI effect. Therefore, the outage probability of the MRC/MRT scheme shows an outage floor at high SNRs. However, to some level a proper choice of α can improve the outage performance of the MRC/MRT scheme. Fig. 3 and 4 illustrate that the outage probability of the system depends on the amount of energy harvested through the receive antenna numbers at the relay, source-relay link distance, and the energy conversion efficiency of the deployed energy harvester at the relay. Moreover, it is significantly influenced by the transmit/receive beamforming design at the relay.

C. Delay-Constrained Throughput

Fig. 5 shows the impact of optimal α on the delay-constrained throughput. As expected, the optimum scheme exhibits the best throughput among all beamforming schemes. The superior performance of the optimum scheme is more pronounced especially between 0.4 and 0.8 values of α. The highest throughput with optimized α for the

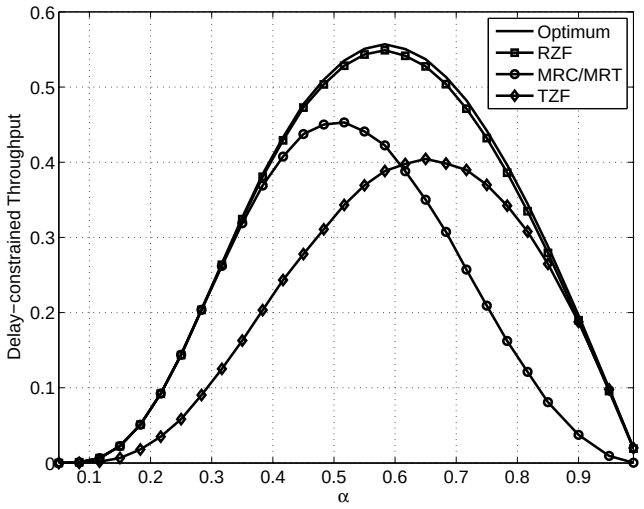

Fig. 5. Delay-constrained throughput of different FD schemes ($M_T = M_R = 3$, $P_S = 10$ dBm, $d_1 = 20$, $d_2 = 10$, $\tau = 3$, $\eta = 0.5$, and $R_c = 2$).

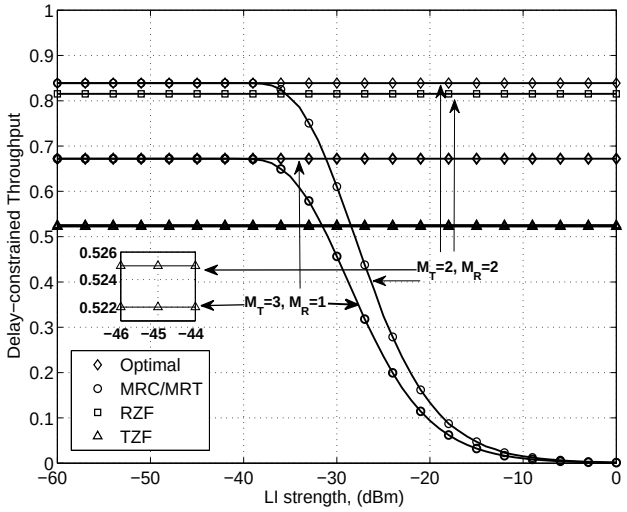

Fig. 6. Delay-constrained throughput versus the LI strength for proposed beamforming schemes with optimal α ($P_S = 20$ dBm, $d_1 = 20$, and $d_2 = 10$).

optimum, RZF, MRC/MRT and TZF schemes are given by 0.557, 0.549, 0.453 and 0.404, respectively. Moreover, we see that each one of the TZF, RZF and MRC/MRT schemes can surpass other beamforming schemes depending on the value of α. This observation reveals the existence of various design choices when performance-complexity tradeoff is considered.

Fig. 6 shows the effect of the LI strength on the delay-constrained throughput when optimum α is used. The total number of antennas is $M_R + M_T = 4$. The ZF-based schemes do not suffer from LI, therefore the delay-constrained transmission throughput remains constant. On the contrary, as expected, the delay-constrained transmission throughput of the MRC/MRT scheme decreases as σ_{RR}^2 and consequently the LI strength increases. When the LI strength is low the ZF-based schemes become inferior as compared to the MRC/MRT scheme. In this region the combination ($M_R = 2$, $M_T = 2$) with MRC/MRT scheme exhibits a near optimum performance. Results, not shown for the configuration ($M_R = 3$, $M_T = 1$), showed inferior performance as compared to the configuration ($M_R = 2$, $M_T = 2$) in all schemes while they showed a superior performance as compared to the configuration ($M_R = 1$, $M_T = 3$). Therefore, performance enhancements can be achieved through equal transmit and receive antenna deployment.

As a final cautionary note we would like to express that the above main findings and insights can be further examined by applying specific RF circuitry and power amplifier model. For example, low efficiency of a RF amplifier used for digital communications can be accounted in a detailed analysis. An implication of such use would be that, often the relay will be unable to operate and the price paid would be a high outage probability due to communication blackout periods. Nevertheless, our results provide useful theoretical performance bounds for the studied system and motivates practical interest from the perspective of wireless-powered full-duplex system implementation.

VII. Conclusion

In this paper, we studied the instantaneous and delay-constrained throughput of a wireless-powered FD MIMO relay system. We designed optimum linear processing at the relay as well as investigated several suboptimum schemes. The optimal time-split for instantaneous throughput maximization of all schemes was derived. We also presented exact and asymptotic closed-form expressions for the outage probability useful to characterize the delay-constrained throughput. We found that the MRC/MRT scheme can offer a higher instantaneous/delay-constrained throughput as compared to the RZF and TZF schemes, when the LI is significantly canceled, and vice versa. The MRC/MRT scheme can provide a better outage performance at low-to-medium SNRs, while the ZF precoders outperform the former at high SNRs.

Appendix A
Proof of Proposition 2

Proof: We show that (18) leads to optimum rank-one solution or such solution can be recovered from the optimum solution that has rank higher than one. First note that instead of solving (16) for a given t, (18) can be solved for a given $y = \bar{y}$. Such optimization problem is expressed as

$$\begin{aligned} \max_{\mathbf{W}_t, t} \quad & t \\ \text{s.t.} \quad & \frac{d_1^\tau}{\rho_1} t\bar{y} \leq \|\mathbf{h}_{SR}\|^2 \bar{y} - \frac{\kappa\rho_1}{d_1^\tau} \|\mathbf{h}_{SR}\|^2 \mathbf{h}_{SR}^\dagger \mathbf{H}_{RR} \mathbf{W}_t \mathbf{H}_{RR}^\dagger \mathbf{h}_{SR} \\ & \bar{y} = \mathsf{tr}\left(\mathbf{W}_t \left(\mathbf{I} + \frac{\kappa\rho_1}{d_1^\tau} \|\mathbf{h}_{SR}\|^2 \mathbf{H}_{RR}^\dagger \mathbf{H}_{RR} \right) \right) \\ & t \leq \frac{\kappa\rho_2}{d_1^\tau d_2^\tau} \|\mathbf{h}_{SR}\|^2 \mathbf{h}_{RD} \mathbf{W}_t \mathbf{h}_{RD}^\dagger \\ & \mathsf{tr}\left(\mathbf{W}_t\right) = 1, \mathbf{W}_t \succeq 0 \end{aligned} \tag{68}$$

where $\bar{y} \in [1, y_{\text{up}}]$. Here, y_{up} is the maximum value of $\bar{y}$ which is the maximum eigenvalue corresponding to $\mathbf{R} \triangleq \mathbf{I} + \frac{\kappa\rho_1}{d_1^\tau} \|\mathbf{h}_{SR}\|^2 \mathbf{H}_{RR}^\dagger \mathbf{H}_{RR}$. The optimum $\mathbf{W}_t$ is the solution that maximizes t for all $y \in [1, y_{\text{up}}]$ for which (68) is feasible.

The optimum $\mathbf{W}_t$ thus obtained will be the same as that obtained by solving (16). The Lagrangian multiplier function for (68) is expressed as

$$\begin{aligned}\mathcal{L}\left(\mathbf{W}_t, t, \{\lambda_i\}_{i=1}^4\right) = -t + \lambda_1 \Bigg(\frac{d_1^\tau}{\rho_1} t\bar{y} - \|\mathbf{h}_{SR}\|^2 \bar{y} \\ + \frac{\kappa\rho_1}{d_1^\tau}\|\mathbf{h}_{SR}\|^2 \mathbf{h}_{SR}^\dagger \mathbf{H}_{RR}\mathbf{W}_t\mathbf{H}_{RR}^\dagger \mathbf{h}_{SR}\Bigg) \\ + \lambda_2\left(\mathrm{tr}\left(\mathbf{W}_t\mathbf{R}\right) - \bar{y}\right) \\ + \lambda_3\left(t - \frac{\kappa\rho_2}{d_1^\tau d_2^\tau}\|\mathbf{h}_{SR}\|^2 \mathbf{h}_{RD}\mathbf{W}_t\mathbf{h}_{RD}^\dagger\right) \\ + \lambda_4\left(\mathrm{tr}(\mathbf{W}_t - 1)\right) - \mathrm{tr}\left(\mathbf{Y}\mathbf{W}_t\right), \qquad (69)\end{aligned}$$

where $\mathbf{Y} \succeq 0$ is the matrix dual variable associated with the constraint $\mathbf{W}_t \succeq 0$. Since (68) is convex and Slater condition holds true, the Karush-Kuhn-Tucker (KKT) conditions are necessary and sufficient for optimality. The KKT conditions for (68) are

$$\begin{aligned}\frac{\partial\mathcal{L}}{\partial\mathbf{W}_t} = 0 \quad \rightarrow \mathbf{Y} = \lambda_1\frac{\kappa\rho_1}{d_1^\tau}\|\mathbf{h}_{SR}\|^2\mathbf{H}_{RR}^\dagger\mathbf{h}_{SR}\mathbf{h}_{SR}^\dagger\mathbf{H}_{RR} \\ +\lambda_2\mathbf{R} + \lambda_4\mathbf{I} - \lambda_3\frac{\kappa\rho_2}{d_1^\tau d_2^\tau}\|\mathbf{h}_{SR}\|^2\mathbf{h}_{RD}^\dagger\mathbf{h}_{RD} \qquad (70)\end{aligned}$$

$$\frac{\partial\mathcal{L}}{\partial t} = 0 \quad \rightarrow \lambda_1\frac{d_1^\tau}{\rho_1}\bar{y} + \lambda_3 = 1 \qquad (71)$$

$$\begin{aligned}\lambda_1\Bigg(\frac{d_1^\tau}{\rho_1}t\bar{y} - \|\mathbf{h}_{SR}\|^2\bar{y} + \frac{\kappa\rho_1}{d_1^\tau} \\ \times\Big\|\mathbf{h}_{SR}\|^2\mathbf{h}_{SR}^\dagger\mathbf{H}_{RR}\mathbf{W}_t\mathbf{H}_{RR}^\dagger\mathbf{h}_{SR}\Bigg) = 0 \qquad (72)\end{aligned}$$

$$\lambda_3\left(t - \frac{\kappa\rho_2}{d_1^\tau d_2^\tau}\|\mathbf{h}_{SR}\|^2\mathbf{h}_{RD}\mathbf{W}_t\mathbf{h}_{RD}^\dagger\right) = 0 \qquad (73)$$

$$\mathrm{tr}\left(\mathbf{W}_t\mathbf{R}\right) - \bar{y} = 0 \qquad (74)$$

$$\mathrm{tr}\left(\mathbf{W}_t\right) - 1 = 0 \qquad (75)$$

$$\mathrm{tr}(\mathbf{Y}\mathbf{W}_t) = 0 \rightarrow \mathbf{Y}\mathbf{W}_t = \mathbf{0}. \qquad (76)$$

The complementary slackness condition (76) means that at KKT optimality, the optimum $\mathbf{W}_t$ lies in the null-space of $\mathbf{Y}$. This means that the rank of $\mathbf{W}_t$ is the nullity of $\mathbf{Y}$. In the following, we analyze the cases in which the optimum $\mathbf{W}_t$ is rank-one (Cases a and c) and not rank-one but the rank-one optimum solution can be recovered from optimum $\mathbf{W}_t$ (Case b).

- Case a: $\lambda_1 = 0, \lambda_3 \neq 0$ - When $\lambda_1 = 0$, the inequality constraint corresponding to (72) is not satisfied with equality, whereas the inequality constraint corresponding to (73) is satisfied with equality since $\lambda_1 = 0$ leads to $\lambda_3 = 1$ (see (71)). In this case, $\mathbf{Y}$ reduces to

$$\begin{aligned}\mathbf{Y} = (\lambda_2 + \lambda_4)\mathbf{I} + \lambda_2\tfrac{\kappa\rho_1}{d_1^\tau}\|\mathbf{h}_{SR}\|^2\mathbf{H}_{RR}^\dagger\mathbf{H}_{RR} - \\ \tfrac{\kappa\rho_2}{d_1^\tau d_2^\tau}\|\mathbf{h}_{SR}\|^2\mathbf{h}_{RD}^\dagger\mathbf{h}_{RD}. \qquad (77)\end{aligned}$$

  It is clear that both λ_2 and λ_4 cannot be equal to zero at optimality. Otherwise, $\mathbf{Y}$ turns to a negative semi-definite matrix contradicting the fact that $\mathbf{Y} \succeq 0$. In all other possible values of λ_2 and λ_4, it is seen that $\mathbf{Z} \triangleq (\lambda_2 + \lambda_4)\mathbf{I} + \lambda_2\frac{\kappa\rho_1}{d_1^\tau}\|\mathbf{h}_{SR}\|^2\mathbf{H}_{RR}^\dagger\mathbf{H}_{RR}$ is a full-rank matrix. Now, we can show that the nullity of $\mathbf{Y}$ cannot be greater than one by contradiction. Assume that $\{\mathbf{u}_{y,q}, q = 1, 2\} \in \mathcal{N}s(\mathbf{Y})$ where $\mathcal{N}s(\mathbf{Y})$ denotes null-space of $\mathbf{Y}$ and let $\mathbf{a}\mathbf{a}^\dagger = \frac{\kappa\rho_2}{d_1^\tau d_2^\tau}\|\mathbf{h}_{SR}\|^2\mathbf{h}_{RD}^\dagger\mathbf{h}_{RD}$. Then,

$$\begin{aligned}\mathbf{Y}\mathbf{u}_{y,q} = \mathbf{Z}\mathbf{u}_{y,q} - \mathbf{a}\mathbf{a}^\dagger\mathbf{u}_{y,q} \\ \rightarrow \mathbf{u}_{y,q} = \mathbf{Z}^{-1}\mathbf{a}\mathbf{a}^\dagger\mathbf{u}_{y,q}, \forall q, \qquad (78)\end{aligned}$$

  which shows that $\mathbf{u}_{y,q}$ is an eigenvector of $\mathbf{Z}^{-1}\mathbf{a}\mathbf{a}^\dagger$ corresponding to eigenvalue 1. Since $\mathrm{rank}(\mathbf{Z}^{-1}\mathbf{a}\mathbf{a}^\dagger) = 1$, it turns out that q cannot take a value greater than 1. This shows that the dimension of null space of $\mathbf{Y}$ is 1, and therefore, the rank of $\mathbf{W}_t$ is one.
- Case b: $\lambda_1 \neq 0, \lambda_3 = 0$ - When optimum $\lambda_3 = 0$, the inequality constraint associated with (72) will be satisfied with equality, whereas that associated with (73) will not be satisfied with equality. Note that $\lambda_3 = 0$ leads to $\lambda_1 = \frac{\rho_1}{d_1^\tau}\frac{1}{\bar{y}}$. In this case, $\mathbf{Y}$ reduces to

$$\begin{aligned}\mathbf{Y} = \tfrac{\rho_1}{d_1^\tau}\tfrac{1}{\bar{y}}\tfrac{\kappa\rho_1}{d_1^\tau}\|\mathbf{h}_{SR}\|^2\mathbf{H}_{RR}^\dagger\mathbf{h}_{SR}\mathbf{h}_{SR}^\dagger\mathbf{H}_{RR} + \\ (\lambda_2 + \lambda_4)\mathbf{I} + \lambda_2\tfrac{\kappa\rho_1}{d_1^\tau}\|\mathbf{h}_{SR}\|^2\mathbf{H}_{RR}^\dagger\mathbf{H}_{RR}. \qquad (79)\end{aligned}$$

  Note that a feasible $\mathbf{Y}$ is the one which has at least a nullity of 1, since the optimum $\mathbf{W}_t$ lies in the null-space of $\mathbf{Y}$. Therefore, at optimality both λ_2 and λ_4 should be zero, otherwise $\mathbf{Y}$ in (79) turns to a full-rank matrix which is not feasible. Consequently, $\mathbf{Y}$ reduces to $\mathbf{Y} = \frac{\rho_1}{d_1^\tau}\frac{1}{\bar{y}}\frac{\kappa\rho_1}{d_1^\tau}\|\mathbf{h}_{SR}\|^2\mathbf{H}_{RR}^\dagger\mathbf{h}_{SR}\mathbf{h}_{SR}^\dagger\mathbf{H}_{RR}$ which is a rank-one matrix. Therefore, the optimum $\mathbf{W}_t$ may not be rank-one. However, we show that optimum rank-one matrix can be recovered from optimum $\mathbf{W}_t$ without loss of optimality.

  Suppose the optimum $\mathbf{W}_t$ has a rank r where $\mathbf{W}_t = \sum_{q=1}^r \sigma_q\mathbf{u}_q\mathbf{u}_q^\dagger$. σ_q and $\mathbf{u}_q, (q = 1, \cdots, r)$ are, respectively, the eigenvalues and eigenvectors of the matrix $\mathbf{W}_t$. Furthermore, due to the equality constraint (75), $\sum_{q=1}^r \sigma_q = 1$. Substituting eigenvalue decomposition of $\mathbf{W}_t$ into the condition (76), we find that

$$\begin{aligned}\sum_{q=1}^r \sigma_q\mathbf{u}_q^\dagger\mathbf{Y}\mathbf{u}_q = 0 \\ \rightarrow \mathbf{u}_q^\dagger\left[\mathbf{H}_{RR}^\dagger\mathbf{h}_{SR}\mathbf{h}_{SR}^\dagger\mathbf{H}_{RR}\right]\mathbf{u}_q = 0, \forall q \qquad (80)\end{aligned}$$

  where the last step is due to the fact that $\mathbf{Y} \succeq 0$. Moreover, following is due to (80)

$$\begin{aligned}\frac{d_1^\tau}{\rho_1}t = \|\mathbf{h}_{SR}\|^2 - \frac{1}{\bar{y}}\frac{\kappa\rho_1}{d_1^\tau}\|\mathbf{h}_{SR}\|^2\mathbf{h}_{SR}^\dagger\mathbf{H}_{RR}\mathbf{W}_t\mathbf{H}_{RR}^\dagger\mathbf{h}_{SR} \\ \rightarrow t = \frac{\rho_1}{d_1^\tau}\|\mathbf{h}_{SR}\|^2. \qquad (81)\end{aligned}$$

  On the other hand, using the eigenvalue decomposition of $\mathbf{W}_t$, the inequality constraint associated with (73) and equality constraint (74), respectively, yield

$$t < \frac{\kappa\rho_2}{d_1^\tau d_2^\tau}\|\mathbf{h}_{SR}\|^2\sum_{q=1}^r \sigma_q\mathbf{u}_q^\dagger\mathbf{h}_{RD}^\dagger\mathbf{h}_{RD}\mathbf{u}_q \qquad (82)$$

$$1 + \frac{\kappa\rho_1}{d_2^\tau}\|\mathbf{h}_{SR}\|^2\sum_{q=1}^r \sigma_q\mathbf{u}_q^\dagger\mathbf{H}_{RR}^\dagger\mathbf{H}_{RR}\mathbf{u}_q = \bar{y}. \qquad (83)$$

  It can be observed from (81) that the optimum value of t does not depend on $\bar{y}$ in the underlying case. An arbitrary $\bar{y}$ where $\bar{y} > 1$ (see (83)) remains optimum. Now we can show that by choosing a particular $\mathbf{u}_q$

from a set $\{\mathbf{u}_q\}_{q=1}^r$ and a specific value of σ_q, (82) is not violated. Consider that $\hat{q} = \max_q \mathbf{u}_q^\dagger \mathbf{h}_{RD}^\dagger \mathbf{h}_{RD} \mathbf{u}_q$. Then, the maximum of (82) is achieved by choosing $\mathbf{u}_{\hat{q}}$ with $\sigma_{\hat{q}} = 1$. This choice does not affect the optimum objective value which remains (81) . As such, the optimum rank-one matrix recovered from $\mathbf{W}_t$ turns to $\sigma_{\hat{q}} \mathbf{u}_{\hat{q}} \mathbf{u}_{\hat{q}}^\dagger$.

- Case c: $\lambda_1 \neq 0, \lambda_3 \neq 0$ - In this case, both the inequality constraints ((72) and (73)) will be satisfied with equality. As such, $\mathbf{Y}$ is given by (70). As long as at least one of λ_2 and λ_4 is non-zero, $\lambda_1 \frac{\kappa\rho_1}{d_1^\tau} \|\mathbf{h}_{SR}\|^2 \mathbf{H}_{RR}^\dagger \mathbf{h}_{SR} \mathbf{h}_{SR}^\dagger \mathbf{H}_{RR} + \lambda_2 \mathbf{R} + \lambda_4 \mathbf{I}$ is a full-rank matrix. On the other hand, $\lambda_3 \frac{\kappa\rho_2}{d_1^\tau d_2^\tau} \|\mathbf{h}_{SR}\|^2 \mathbf{h}_{RD}^\dagger \mathbf{h}_{RD}$ is a rank-one matrix. Consequently, as in Case a, the optimum $\mathbf{W}_t$ can be shown to be a rank-one matrix. Therefore, it is sufficient to show that both λ_2 and λ_4 cannot be zero at the optimality. Towards this end, we use the method of contradiction. Assume that $\lambda_2 = 0$ and $\lambda_4 = 0$. Then, $\mathbf{Y}$ reduces to

$$\begin{aligned}\mathbf{Y} \quad &= \lambda_1 \tfrac{\kappa\rho_1}{d_1^\tau} \|\mathbf{h}_{SR}\|^2 \mathbf{H}_{RR}^\dagger \mathbf{h}_{SR} \mathbf{h}_{SR}^\dagger \mathbf{H}_{RR} \\ &\quad - \lambda_3 \tfrac{\kappa\rho_2}{d_1^\tau d_2^\tau} \|\mathbf{h}_{SR}\|^2 \mathbf{h}_{RD}^\dagger \mathbf{h}_{RD}. \end{aligned} \tag{84}$$

Note that $\mathbf{Y}$ should be positive-semidefinite. Since $\mathbf{Y}$ in (84) is the difference between two rank-one matrices, it can be readily shown from Weyl's inequalities for eigenvalues of sum of Hermitian matrices that $\mathbf{Y}$ cannot remain positive-semidefinite except in the case with $\lambda_3 \frac{\kappa\rho_2}{d_1^\tau d_2^\tau} \|\mathbf{h}_{SR}\|^2 \mathbf{h}_{RD}^\dagger \mathbf{h}_{RD} = 0$, i.e., $\lambda_3 = 0$ for non-zero $\mathbf{h}_{SR}$ and $\mathbf{h}_{RD}$. This contradicts with the assumption $\lambda_3 \neq 0$, which consequently contradicts the assumption that both λ_2 and λ_4 are zero. This completes the proof of the proposition. ∎

Appendix B
Proof of Proposition 5

Applying the series expansion of $\gamma(a,x)$ and $\Gamma(a,x)$ [29, Eq. (8.354.1) and (8.354.2)] we have

$$\begin{aligned} F_{\gamma_{\mathsf{TZF}}}(z) &= 1 - \frac{1}{\Gamma(M_R)} \int_{\frac{d_1^\tau z}{\rho_1}}^\infty \left(1 - \frac{1}{\Gamma(M_T - 1)} \right. \\ &\quad \left. \times \sum_{k=0}^\infty \frac{(-1)^k}{k!(k+M_T)} \left(\frac{d_1^\tau d_2^\tau}{\kappa\rho_2} \frac{z}{x}\right)^{M_T+k-1} \right) x^{M_R-1} e^{-x} dx, \\ &= 1 - \frac{\Gamma\left(M_R, \frac{d_1^\tau z}{\rho_1}\right)}{\Gamma(M_R)} + \frac{1}{\Gamma(M_T-1)\Gamma(M_R)} \\ &\quad \times \sum_{k=0}^\infty \frac{(-1)^k}{k!(k+M_T)} \left(\frac{d_1^\tau d_2^\tau}{\kappa} \frac{z}{\rho_2}\right)^{M_T+k-1} \mathcal{I}(k), \end{aligned} \tag{85}$$

where $\mathcal{I}(k) = \int_{\frac{d_1^\tau z}{\rho_1}}^\infty x^{M_R - M_T - k} e^{-x} dx$, that has closed form solution given by

$$\mathcal{I}(k) = \begin{cases} \left(\frac{d_1^\tau z}{\rho_1}\right)^{M_R - M_T - k + 1} E_{M_T - M_R + k}\left(\frac{d_1^\tau z}{\rho_1}\right), \\ \qquad M_T > M_R - k \\ \left(\frac{d_1^\tau z}{\rho_1}\right)^{M_R - M_T - k + 1} \alpha_{M_R - M_T - k}\left(\frac{d_1^\tau z}{\rho_1}\right), \\ \qquad M_T \leq M_R - k \end{cases} \tag{86}$$

where $\alpha_n(x) = \int_1^\infty x^n e^{-x} dx$ [30, Eq. (5.1.5)]. By substituting (86) into (85), and then applying [30, Eq. (5.1.8)] and [30, Eq. (5.1.12)], we get (87) at the top of the next page where $\psi(1) = -0.57721...$ and $\psi(n) = \psi(1) + \sum_{m=1}^{n-1} \frac{1}{m}$, for $n > 1$ [29, Eq. (9.73)]. In the high SNR regime, i.e., $\rho_1, \rho_2 \to \infty$, omitting higher order items of the series expansion in (87), the desired result follows after some simple algebraic manipulations.

Appendix C
Proof of Proposition 6

Using the series expansion of $\gamma(a,x)$ and $\Gamma(a,x)$, we get

$$\begin{aligned} F_{\gamma_{\mathsf{RZF}}}(z) &= 1 - \frac{\Gamma\left(M_R, \frac{d_1^\tau z}{\rho_1}\right)}{\Gamma(M_R)} + \frac{1}{\Gamma(M_R)\Gamma(M_T)} \\ &\quad \sum_{k=0}^\infty \frac{(-1)^k}{k!(k+M_T)} \left(\frac{d_1^\tau d_2^\tau}{\kappa} \frac{z}{\rho_2}\right)^{M_T+k} \mathcal{I}_1(k) + \\ &\quad \frac{1}{\Gamma(M_R)} \left(\frac{d_1^\tau z}{\rho_1}\right)^{M_R-1} \left(e^{-\frac{d_1^\tau z}{\rho_1}} - \frac{1}{\Gamma(M_T)} \right. \\ &\quad \left. \sum_{k=0}^\infty \frac{(-1)^k}{k!(k+M_T)} \left(\frac{d_1^\tau d_2^\tau}{\kappa} \frac{z}{\rho_2}\right)^{M_T+k} \mathcal{I}_2(k) \right), \end{aligned} \tag{88}$$

where $\mathcal{I}_1(k) = \int_{\frac{d_1^\tau z}{\rho_1}}^\infty x^{M_R - M_T - k - 1} e^{-x} dx$ is evaluated as

$$\mathcal{I}_1(k) = \begin{cases} \left(\frac{d_1^\tau z}{\rho_1}\right)^{M_R - M_T - k} E_{M_T - M_R + k + 1}\left(\frac{d_1^\tau z}{\rho_1}\right), \\ \qquad M_T > M_R - k - 1 \\ \left(\frac{d_1^\tau z}{\rho_1}\right)^{M_R - M_T - k} \alpha_{M_R - M_T - k - 1}\left(\frac{d_1^\tau z}{\rho_1}\right), \\ \qquad M_T \leq M_R - k - 1 \end{cases} \tag{89}$$

and $\mathcal{I}_2(k) = \int_{\frac{d_1^\tau z}{\rho_1}}^\infty x^{-M_T - k} e^{-x} dx$ is solved as

$$\mathcal{I}_2(k) = \left(\frac{d_1^\tau z}{\rho_1}\right)^{-M_T - k + 1} E_{M_T + k}\left(\frac{d_1^\tau z}{\rho_1}\right). \tag{90}$$

Substituting (89) and (90) into (88), and expanding the result with the help of [30, Eq. (5.1.8) and Eq. (5.1.12)], and then only selecting the sufficient and ignoring the higher order terms, we arrive at (51).

Appendix D
Proof of Proposition 7

Let $Z_3 = \| \boldsymbol{h}_{SR} \|^2 |h_{RD}|^2$, and observing that X_2 and Z_3 are independent, we have

$$F_{\gamma_{\mathsf{MRC}}^{\mathsf{low}}}(z) = 1 - F_{X_2}\left(\frac{1}{\kappa\sigma_{RR}^2} \frac{1}{z}\right) \left(1 - F_{Z_3}\left(\frac{d_1^\tau d_2^\tau}{\kappa\rho_2} z\right)\right), \tag{91}$$

where $F_{X_2}(\cdot)$ is given in (56) and the cdf of Z_3 can be derived as

$$\begin{aligned} F_{Z_3}(z) &= \int_0^\infty \Pr\left(|h_{RD}|^2 < \frac{z}{x}\right) f_{\|\boldsymbol{h}_{SR}\|^2}(x) dx, \\ &= 1 - \frac{2}{\Gamma(M_R)} z^{\frac{M_R}{2}} K_{M_R}(2\sqrt{z}), \end{aligned} \tag{92}$$

where we used [29, Eq. (3.471.9)] to derive (92). Finally, substituting (56) and (92) into (91) yields the desired result.

$$F_{\gamma_{\mathrm{TZF}}}(z)=1-\frac{\Gamma\left(M_R,\frac{d_1^\tau z}{\rho_1}\right)}{\Gamma(M_R)}+\frac{1}{\Gamma(M_T-1)\Gamma(M_R)}\left(\frac{d_1^\tau z}{\rho_1}\right)^{M_R}\sum_{k=0}^{\infty}\frac{(-1)^k}{k!(k+M_T)}\left(\frac{\sigma_D^2}{\sigma_R^2}\frac{d_2^\tau}{\kappa}\right)^{M_T+k-1}$$
$$\times\begin{cases}\left(\frac{(-1)^{M_T-M_R+k-1}}{\Gamma(M_T-M_R+k)}\left(\frac{d_1^\tau z}{\rho_1}\right)^{M_T-M_R+k-1}\left(-\ln\left(\frac{d_1^\tau z}{\rho_1}\right)+\psi(M_T-M_R+k)\right)\right. & \\ \left.-\sum\limits_{\substack{\ell=0\\ \ell\neq M_T-M_R+k-1}}^{\infty}\frac{(-1)^\ell}{\ell+M_R-M_T-k+1}\left(\frac{d_1^\tau z}{\rho_1}\right)^{\ell}\right), & M_T>M_R-k\\ \Gamma(M_R-M_T-k+1)\left(\frac{d_1^\tau z}{\rho_1}\right)^{M_T-M_R-k-1} & \\ \quad\times e^{-\frac{d_1^\tau z}{\rho_1}}\left(1+\frac{d_1^\tau z}{\rho_1}+\frac{1}{2!}\left(\frac{d_1^\tau z}{\rho_1}\right)^2+\cdots+\frac{1}{(M_R-M_T-k)!}\left(\frac{d_1^\tau z}{\rho_1}\right)^{M_R-M_T-k}\right), & M_T\leq M_R-k\end{cases}\tag{87}$$

REFERENCES

[1] A. Sabharwal *et al.*, "In-band full-duplex wireless: Challenges and opportunities," *IEEE J. Sel. Areas Commun.*, vol. 32, pp. 1637-1652, Sep. 2014.

[2] B. P. Day, A. R. Margetts, D. W. Bliss, and P. Schniter, "Full-duplex MIMO relaying: Achievable rates under limited dynamic range," *IEEE J. Sel. Areas Commun.*, vol. 30, pp. 1541-1553, Sep. 2012.

[3] T. Riihonen, S. Werner, and R. Wichman, "Hybrid full-duplex/half-duplex relaying with transmit power adaptation," *IEEE Trans. Wireless Commun.*, vol. 10, pp. 3074-3085, Sep. 2011.

[4] T. Riihonen, S. Werner, and R. Wichman, "Mitigation of loopback self-interference in full-duplex MIMO relays," *IEEE Trans. Signal Process.*, vol. 59, pp. 5983-5993, Dec. 2011.

[5] M. Duarte, "Full-duplex wireless: Design, implementation and characterization," *Ph.D. dissertation*, Dept. Elect. and Computer Eng., Rice University, Houston, TX, 2012.

[6] D. Korpi, T. Riihonen, V. Syrjala, L. Anttila, M. Valkama, and R. Wichman, "Full-duplex transceiver system calculations: Analysis of ADC and linearity challenges," *IEEE Trans. Wireless Commun.*, vol. 13, pp. 3821-3836, July 2014.

[7] E. Aryafar, M. A. Khojastepour, K. Sundaresan, S. Rangarajan and M. Chiang, "MIDU: Enabling MIMO full-duplex," in *Proc.* 18*th Annual Intl. Conf. Mobile Computing and Networking (MobiCom 2012)*, Istanbul, Turkey, Aug. 2012, pp. 257-268.

[8] H. A. Suraweera, I. Krikidis, G. Zheng, C. Yuen and P. J. Smith, "Low-complexity end-to-end performance optimization in MIMO full-duplex relay systems," *IEEE Trans. Wireless Commun.*, vol. 13, pp. 913-927, Feb. 2014.

[9] H. Q. Ngo, H. A. Suraweera, M. Matthaiou and E. G. Larsson, "Multipair full-duplex relaying with massive arrays and linear processing," *IEEE J. Sel. Areas Commun.*, vol. 32, pp. 1721-1737, Sep. 2014.

[10] B. Medepally and N. B. Mehta, "Voluntary energy harvesting relays and selection in cooperative wireless networks," *IEEE Trans. Wireless Commun.*, vol. 9, pp. 3543-3553, Nov. 2010.

[11] Z. Ding, C. Zhong, D. W. K. Ng, M. Peng, H. A. Suraweera, R. Schober and H. V. Poor, "Application of smart antenna technologies in simultaneous wireless information and power transfer," *IEEE Commun. Mag.,* vol. 53, pp. 86-93, Apr. 2015.

[12] K. Huang and X. Zhou, "Cutting last wires for mobile communication by microwave power transfer," *IEEE Commun. Mag.*, vol. 53, pp. 86-93, June 2015.

[13] R. Zhang and C. Ho, "MIMO broadcasting for simultaneous wireless information and power transfer," *IEEE Trans. Wireless Commun.*, vol. 12, pp. 1989-2001, May 2013.

[14] L. R. Varshney, "Transporting information and energy simultaneously," in *Proc. IEEE Intl. Symp. Inf. Theory (ISIT 2008)*, Toronto, Canada, Jul. 2008, pp. 1612-1616.

[15] P. Grover and A. Sahai, "Shannon meets Tesla: wireless information and power transfer," in *Proc. IEEE Intl. Symp. Inf. Theory (ISIT 2010)*, Austin, TX, June 2010, pp. 2363-2367.

[16] X. Zhou, R. Zhang, and C. K. Ho, Wireless information and power transfer: Architecture design and rate-energy tradeoff," *IEEE Trans. Commun.*, vol. 61, pp. 4757-4767, Nov. 2013.

[17] Z. Ding, S. M. Perlaza, I. Esnaola, and H. V. Poor, "Power allocation strategies in energy harvesting wireless cooperative networks," *IEEE Trans. Wireless Commun.*, vol. 13, pp. 846-860, Feb. 2014.

[18] D. W. K. Ng, E. S. Lo, and R. Schober, "Wireless information and power transfer: Energy efficiency optimization in OFDMA systems," *IEEE Trans. Wireless Commun.*, vol. 12, pp. 6352-6370, Dec. 2013.

[19] A. A. Nasir, X. Zhou, S. Durrani, and R. Kennedy, "Relaying protocols for wireless energy harvesting and information processing," *IEEE Trans. Wireless Commun.*, vol. 12, pp. 3622-3636, Jul. 2013.

[20] A. A. Nasir, X. Zhou, S. Durrani and R. A. Kennedy, "Wireless-powered relays in cooperative communications: Time-switching relaying protocols and throughput analysis," *IEEE Trans. Commun.*, vol. 63, pp. 1607-1622, May 2015.

[21] H. Chen, Y. Li, J. L. Rebelatto, B. F. Uchôa-Filho, and B. Vucetic, " Harvest-Then-Cooperate: Wireless-Powered Cooperative Communications," *IEEE Trans. Signal Process.*, vol. 63, pp. 1700-1711, Apr. 2015.

[22] I. Krikidis, "Simultaneous information and energy transfer in large scale networks with/without relaying," *IEEE Trans. Commun.*, vol. 62, pp. 900-912, Mar. 2014.

[23] I. Krikidis, S. Sasaki, S. Timotheou, and Z. Ding, "A low complexity antenna switching for joint wireless information and energy transfer in MIMO relay channels," *IEEE Trans. Commun.*, vol. 62, pp. 1577-1587, May 2014.

[24] G. Zhu, C. Zhong, H. A. Suraweera, G. K. Karagiannidis, Z. Zhang, and T. A. Tsiftsis,"Wireless information and power transfer in relay systems with multiple antennas and interference," *IEEE Trans. Commun.*, vol. 63, pp. 1400-1418, Apr. 2015.

[25] H. Ju and R. Zhang, "Optimal resource allocation in full-duplex wireless powered communication network," *IEEE Trans. Commun.*, vol. 62, pp. 3528-3540, Oct. 2014.

[26] K. Yamazaki, Y. Sugiyama, Y. Kawahara, S. Saruwatari, and T. Watanabe, "Preliminary evaluation of simultaneous data and power transmission in the same frequency channel," in *Proc. IEEE WCNC 2015*, New Orleans, LA, Mar. 2015, pp. 1-6.

[27] C. Zhong, H. A. Suraweera, G. Zheng, I. Krikidis, and Z. Zhang, "Wireless information and power transfer With full duplex relaying," *IEEE Trans. Commun.*, vol. 62, pp. 3447-3461, Oct. 2014.

[28] Y. Zeng and R. Zhang, "Full-duplex wireless-powered relay with self-energy recycling," *IEEE Wireless Commun. Lett.*, vol. 4, pp. 201-204, Apr. 2015.

[29] I. S. Gradshteyn and I. M. Ryzhik, *Table of Integrals, Series and Products*. 7th ed. Academic Press, 2007.

[30] M. Abramowitz and I. A. Stegun, *Handbook of Mathematical Functions With Formulas, Graphs, and Mathematical Tables*. 9th ed. New York: Dover, 1970.

[31] X. Zhou, R. Zhang, and C. Ho, "Wireless information and power transfer: Architecture design and rate-energy tradeoff," *IEEE Trans. Commun.,* vol. 61, pp. 4757-4767, Nov. 2013.

[32] A. Masmoudi, and T. Le-Ngoc, "Residual self-interference after cancellation in full-duplex systems," in *Proc. IEEE Intl. Conf. Commun. (ICC 2014),* Sydney, Australia, June 2014, pp. 4680-4685.

[33] A. C. Cirik, Y. Rong, and Y. Hua, "Achievable rates of full-duplex MIMO radios in fast fading channels with imperfect channel estimation," *IEEE Trans. Signal Process.,* vol. 62, pp. 3874-3886, Aug. 2014.

[34] G. Auer et al., "How much energy is needed to run a wireless network?," *IEEE Wireless Commun. Mag.*, vol.18, pp. 40-49, Oct. 2011.

[35] F. Dostal, "New advances in energy harvesting power conversion," Analog Devices, vol. 49, Sep. 2015. Available: http://www.analog.com/library/analogdialogue/archives/4909/energy-harvesting.html.

[36] R. A. Horn and C. A. Johnson, *Matrix Analysis.* Cambridge Univ. Press, 2nd Ed., New York, NY: 2013.
[37] W. W. Hager, "Updating the inverse of a matrix," *SIAM Review,* vol. 31, no. 2, pp. 221-239, June 1989.
[38] R. V. Hogg and A. T. Craig, *Introduction to Mathematical Statistics*. 4th ed. Macmillan, New York, 1978.
[39] "3GPP Technical Specication Group Radio Access Network, Evolved Universal Terrestrial Radio Access (E-UTRA): Further Advancements for E-UTRA Physical Layer Aspects" (Release 9), 3GPP Std. TS 36.814 V9.0.0, 2010.